NACA

RESEARCH MEMORANDUM

AN AUTOPILOT-DETERMINED TRANSONIC LIFT AND DRAG CHARACTERISTICS OF THE YF-102 AIRPLANE WITH TWO WING CONFIGURATIONS

By Edwin J. Saltzman, Donald R. Bellman,
and Norman T. Musialowski

High-Speed Flight Station
Edwards, Calif.

NATIONAL ADVISORY COMMITTEE
FOR AERONAUTICS

WASHINGTON

July 20, 1956
Declassified January 12, 1961

NATIONAL ADVISORY COMMITTEE FOR AERONAUTICS

RESEARCH MEMORANDUM

FLIGHT-DETERMINED TRANSONIC LIFT AND DRAG CHARACTERISTICS OF THE YF-102 AIRPLANE WITH TWO WING CONFIGURATIONS

By Edwin J. Saltzman, Donald R. Bellman,
and Norman T. Musialowski

SUMMARY

Lift and drag characteristics of the Convair YF-102 airplane have been determined in flight for the symmetrical wing configuration and for the cambered wing configuration. The data were obtained for lift coefficients between 0.025 and 0.73, for altitudes of 25,000 feet, 40,000 feet, and 50,000 feet and for Mach numbers from 0.6 to 1.17.

The results indicated that the lift-curve slopes increased gradually with lift over the lift range from 0.1 to 0.4 with much greater increase for the symmetrical wing configuration than for the cambered wing configuration. In addition, the modifications comprising the cambered configuration caused the angle of attack for zero lift to increase less than 0.5°.

The cambered configuration experienced lower drag coefficient values for lift coefficient values above 0.1. Maximum advantage of the cambered configuration was realized at lift coefficients of 0.3 and above, where the reduction in drag coefficient amounted to about 0.01. The drag-due-to-lift values for the cambered configuration were 65 to 75 percent of the symmetrical values at a lift coefficient of 0.2 and for Mach number values below the drag rise. At a lift coefficient value of 0.35 the drag-due-to-lift of the cambered wing was 75 to 85 percent of the symmetrical wing values. The maximum lift-drag ratio for the cambered wing was almost 20 percent higher than for the comparable symmetrical wing values throughout the Mach number range.

Comparisons of flight and tunnel drag characteristics suggest a tendency of zero-lift drag coefficient to decrease with increasing Reynolds number; however, it cannot be determined from these comparisons what part of the zero-lift drag coefficient change is a result of Reynolds number and what portion should be attributed to model variations from exact reproductions, or to inaccuracies in the data.

INTRODUCTION

The NACA High-Speed Flight Station at Edwards, Calif. has made a flight determination of the lift and drag characteristics of the Convair YF-102 airplane. The airplane was first flown with a symmetrical section wing; then, cambered leading edges, reflexed tips, and a second pair of fences were attached to the wings and additional flights were made. This paper presents the lift and drag characteristics of the airplane with both wing configurations. The tests were conducted at altitudes of 25,000 feet and 40,000 feet, covering the Mach number range from 0.6 to approximately 1.17 and the lift-coefficient range from 0.025 to 0.73. In addition, a small amount of data with the cambered wing configuration was obtained at an altitude of 50,000 feet. The tests were made from December 1954 to June 1955. Comparison is also made with unpublished 1/20-scale model data from the NACA Langley 8-foot transonic wind tunnel. These model data, prepared by Robert S. Osborne and Kenneth E. Tempelmeyer, represent both the cambered and symmetrical configurations.

SYMBOLS

A	airplane cross-sectional area, sq ft
A	aspect ratio
A_3	tail pipe exit area (engine cold), sq ft
a_l	longitudinal acceleration, g units
a_n	normal acceleration, g units
$b/2$	wing semispan, ft
C_D	drag coefficient, D/qS
C_{D_0}	zero-lift drag coefficient
C_f	thrust coefficient, $\frac{\text{Thrust measured by thrust stand}}{\text{Thrust determined by probe measurements}}$
C_L	lift coefficient, L/qS

C_{L_α} lift-curve slope, deg^{-1} or radians^{-1}

C_N normal-force coefficient, Wa_n/qS

C_X longitudinal-force coefficient, $\frac{F_n - Wa_l}{qS}$

$\bar{c}$ mean aerodynamic chord, ft

D drag force along flight path, lb

ΔC_D increment in drag coefficient, $C_D - C_{D_{O_s}}$, (where $C_{D_{O_s}}$ is adjusted for change in area when deriving ΔC_D for cambered wing)

$\Delta C_D/C_L{}^2$ drag-due-to-lift factor

F_j jet thrust, lb

F_n net thrust, lb

F_r ram drag, lb

g gravitational acceleration, ft/sec^2

h_p pressure altitude, ft

I_X moment of inertia about X-axis, slug-ft^2

I_Y moment of inertia about Y-axis, slug-ft^2

I_Z moment of inertia about Z-axis, slug-ft^2

I_{XZ} product of inertia, slug-ft^2

L lift force normal to flight path, lb

$(L/D)_{max}$ maximum lift-drag ratio

l fuselage length, ft

M	Mach number
N	high-pressure compressor speed, rpm
p	static pressure, lb/ft^2
p'	total pressure, lb/ft^2
q	dynamic pressure, $0.7M^2p$, lb/ft^2
S	wing area, sq ft
T	total temperature, ^oR
V	airplane velocity, ft/sec
W	airplane weight, lb
w_a	engine air flow, lb/sec
x	distance along fuselage from fuselage zero length station, ft
α	angle of attack, deg
δ_e	elevon deflection, $\frac{\delta_{e_L} + \delta_{e_R}}{2}$, deg

Subscripts:

L	left
R	right
0	free stream
1	duct station approximately 5 feet from inlet
2	compressor face station
3	exhaust exit station
c	cambered
s	symmetrical

AIRPLANE AND MODELS

Airplane

The Convair YF-102 airplane is a single-engine, 60° delta-wing interceptor powered by a J57-P-11 turbojet engine having an installed sea-level thrust of approximately 11,300 pounds with afterburner, or 7,400 pounds without afterburner. This airplane weighs approximately 28,000 pounds at take-off, resulting in a maximum take-off thrust-weight ratio of about 0.4. The YF-102 does not have a horizontal tail, but utilizes elevons at the wing trailing edges for longitudinal control. These controls comprise almost 10 percent of the wing area, and therefore can produce large drag contributions.

The two airplane configurations tested are designated in this paper as the symmetrical wing and the cambered wing, however they also differed in several other respects. The symmetrical wing had a maximum thickness of 4 percent of the chord and had a single pair of fences located at 67 percent semispan, extending from the leading edge to the elevon hinge line. The cambered wing was a modification of the symmetrical wing. Cambered leading edges were installed and the existing fences were extended forward around the leading edge. A second pair of fences was mounted at 37 percent semispan, and the wing tips were reflexed 10° up at the trailing edge outboard of the elevon (82 percent semispan). The leading-edge modification consisted of a conical camber extending from root to tip with a parabolic distribution over the outboard 6.4 percent local semispan. This leading-edge addition decreased the wing thickness ratio to 0.039 at the root and to 0.035 at the outboard edge of the elevon, and also increased the wing area by about 5 percent.

Figure 1 presents three-view drawings of the two configurations and figure 2 shows three general views of the airplane. A photograph illustrates the cambered wing leading edge in figure 3; details of this leading edge are shown in figure 4. General physical characteristics of the airplane are given in table I. The area-rule concept was not incorporated in the design of this airplane; however the normal area distribution is shown in figure 5.

Wind-Tunnel Models

Differences exist between the full-scale airplanes and the wind-tunnel models used for comparison. For both models the fuselage diameter was 0.2 inch smaller and the fuselage tail cone was about 1.1 inches shorter and 0.3 inch larger in diameter than a true 1/20-scale model. The base convergence angle was about the same for the model and the

full-scale airplanes. In addition, the symmetrical wing model had a shortened fuselage nose and the cambered wing model did not have fences at 37 percent semispan.

INSTRUMENTATION

The YF-102 airplane contained standard NACA recording instruments and synchronizing timer for measuring all quantities pertinent to the reduction of lift and drag data except for the fuel meter (for establishing center-of-gravity location) which was read by the pilot, and the compressor speed indicator which was photographed by a 35-millimeter movie camera operating at 2 frames per second.

An NACA standard airspeed head provided total pressure and static pressure from points 87 inches and 79 inches, respectively, forward of the fuselage zero length station. Angle of attack was measured by a vane at a point about 64 inches ahead of the fuselage zero length station. Total air temperature was measured by a shielded resistance-type probe located beneath the fuselage nose.

Total pressure at the compressor face during the cambered wing flights was obtained by 6 radial rakes of 5 probes each located immediately ahead of the compressor. These probes recorded individually on separate cells and it was noted that two widely separated probes, when averaged, gave results equal to the average of all 30 probes over the Mach number and angle-of-attack ranges. Subsequently, these two probes provided total pressure p'_2 which was used to evaluate ram drag for for the remainder of the study. Engine exit total pressure was measured by an air-cooled probe located at the nozzle exit plane of the afterburner.

CALCULATIONS AND METHODS

The net thrust of the engine was determined by using the equations:

$$F_n = F_j - F_r$$

$$F_j = C_f A_3 (1.259 p'_3 - p_0)$$

$$F_r = \frac{V_0 w_a}{g}$$

The nozzle coefficient C_f was determined from a ground thrust-stand measurement and is shown in figure 6. It was necessary to extrapolate the curve because higher pressure ratios are attainable at altitude than can be obtained on the ground. The tail pipe total pressure was measured with the probe mentioned in the previous section and ambient pressure was determined from the altitude measuring system. Airplane velocity V_0 was calculated from the airplane Mach number and the outside air total temperature. Air flow w_a was determined from engine compressor characteristic curves adjusted to flight conditions by total temperature and total pressure. Total temperature T_2 was assumed to be the same as outside air total temperature. The method of determining total pressure p'_2 during the cambered wing configuration tests has been described in the previous section, but during the tests covering the symmetrical wing configuration the probes at the compressor face, station 2, were not available. However, duct total pressure was recorded by a rake located at station 1 (approximately 5 ft from inlet) and it was found during the cambered wing tests that the ratio of total pressure measured at the duct station to total pressure measured at compressor face station p'_1/p'_2 varied in a regular and consistent manner with compressor speed N. Thus, sufficiently accurate values of compressor face total pressure were available for the symmetrical wing tests.

Accelerometers were used to evaluate the lift and drag forces and the resultant normal and longitudinal coefficients were used in the equations:

$$C_L = C_N \cos \alpha - C_X \sin \alpha$$

$$C_D = C_X \cos \alpha + C_N \sin \alpha$$

ACCURACY

The angle of attack as measured by the vane was checked during seven carefully executed, level, unaccelerated runs by comparing the vane readings with those indicated by the longitudinal accelerometer. The average difference was about 0.25°. This error is probably a combination of upwash, vane floating, and boom air-load effects (effects of pitching velocity and boom acceleration loads were removed). The upwash caused by the wing was calculated by the method of reference 1 and was found to be about 0.04° at a Mach number of 0.8 and at an altitude of 40,000 feet. The upwash from the boom and fuselage was calculated by the method of reference 2 and was found to be 0.12° for the same conditions.

The following table shows the magnitudes of error in lift coefficient and drag coefficient which result from the inability to obtain exact measurements of certain pertinent quantities. This table is calculated for level flight at $M \approx 0.8$; $h_p \approx 40{,}000$ feet, giving a lift coefficient of approximately 0.2. At higher Mach numbers or lower altitudes, or both, resultant ΔC_L and ΔC_D values would become smaller.

Error source	Accuracy of error source	Resultant ΔC_L	Resultant ΔC_D
1. W, lb	±100 maximum	Negligible	±0.0001
2. a_n, g	±0.05 maximum	±0.010	±0.0010
3. a_l, g	±0.005 maximum	Negligible	±0.0010
4. F_n, lb	±100 maximum	Negligible	±0.0008
5. q, lb/ft^2	±4.5 maximum	±0.005	±0.0005
6. α, deg	±0.25 average	Negligible	±0.0009

The error in dynamic pressure q is based on $\Delta M = 0.01$ determined by the NACA radar calibration technique of reference 3.

It should be mentioned that estimated errors 1 to 5 represent the maximum discrepancies these sources can contribute for $M \approx 0.8$; $h_p \approx 40{,}000$ feet, and that maximum errors calculated for 25,000 feet would be about half as large. There was no distinguishable difference between the scatter of data for 40,000 feet and for 25,000 feet. Thus, it appears the magnitudes of the individual errors range at random between their limits, tending to cancel one another. This condition results in the actual scatter being considerably less than the sum of estimated errors 1 to 6, as shown by the data of figure 8 where the maximum scatter in drag coefficient is about ±0.0020 for $C_L \leqq 0.2$ and $M < 0.9$. Because these data are subsequently faired, the resulting relationship of drag coefficient to lift coefficient is virtually void of random error at low and moderate lift values where ample data points are obtained. Since all summary data are derived from faired basic data, it is estimated that the error in drag coefficient at $C_L \leqq 0.2$ and in the subsonic region is within 0.0010. The error in drag coefficient due to $\Delta\alpha$ varies directly with lift, consequently the net error will vary upward or downward as lift coefficient varies from 0.2.

TESTS AND PRESENTATION OF DATA

The data presented in this paper were obtained during wind-up turns, push-overs, and level runs at altitudes of 25,000 feet and 40,000 feet. In addition a small amount of data was obtained at high lift conditions with the cambered wing configuration at an altitude of 50,000 feet. The Mach number range of the tests extended from 0.6 to 1.17. The Reynolds number based on mean aerodynamic chord varied from 23×10^6 to 77×10^6. During the program the airplane lift range was limited between normal acceleration values of 0.25g to 3.7g. The center-of-gravity position for the tests was about 29 percent mean aerodynamic chord.

The basic flight data for both the cambered and symmetrical wing configurations are presented in figures 7 and 8, which show plots of lift coefficient against angle of attack and drag coefficient against lift coefficient for selected constant Mach numbers. Data from the three altitude levels, with afterburner on and afterburner off, have been used indiscriminately because no significant differences could be attributed to these conditions. Two probes located in the fuselage base annulus substantiated the fact that there was no significant change in base drag between afterburner-on and afterburner-off conditions.

The data of figures 7 and 8 are for trim conditions and it should be realized there is considerable variation of lift and drag with trim because of the effects of the elevons. Figure 9 shows the variation of elevon deflection for trim with both Mach number and lift for the cambered and symmetrical wing configurations.

DISCUSSION OF RESULTS

Lift

Comparison of figures 7(a) and 7(b) indicates that the extrapolated angle of attack for zero lift was less than 0.5° larger for the cambered wing configuration than for the symmetrical wing configuration. Figure 7 also shows that as the lift coefficient increases from 0.1 to 0.4, there is a noticeable increase in lift-curve slope that is greater for the symmetrical wing configuration than for the cambered wing configuration, and that the change in lift-curve slope occurs gradually over a considerable range of lift coefficient. Figure 10 compares the lift-curve slopes of the two configurations at C_L values of 0.1 and 0.3.

Drag

Before a discussion of drag is attempted, it should be mentioned that all drag differences between the two configurations do not result solely from camber but are caused by the combined effects of all the configuration changes and the resultant trim changes. In addition, it should be noted that the wing areas for the two configurations are different and that the lift and drag coefficients for each configuration have been calculated using the corresponding wing area.

Values of drag coefficient for zero lift, extrapolated from the low-lift data of figure 8, are shown in figure 11. The drag-rise Mach number, when defined as the Mach number where $\frac{dC_D}{dM} = 0.1$, is approximately 0.93 for both configurations and the supersonic drag coefficient level is about three times the zero-lift drag coefficient prior to the drag rise.

A comparison of the basic plots of drag coefficient against lift coefficient at constant Mach number for both the cambered and symmetrical wing configurations indicates a less rapid increase in drag coefficient with lift coefficient for the cambered wing throughout the Mach number range. The comparison can be seen more clearly in figure 12 in which data from the two configurations are shown on the same plot for three representative Mach numbers in the subsonic and transonic speed ranges. The maximum advantage of the cambered wing configuration occurs at lift coefficients above 0.3 and amounts to a decrease in drag coefficient of about 0.01 at a lift coefficient of 0.3.

A measure of the drag resulting from lift is the slope of the curves of C_L^2 plotted against C_D as shown in figure 13. It can be seen that the slopes are not constant over the tested lift range of the airplane but that variations occur, particularly for the cambered wing configuration. Because of the nonlinearity of the C_D, C_L^2 relationship for the cambered wing, the parameter $\Delta C_D/C_L^2$ is used as a drag-due-to-lift factor to form a basis for comparison of the two configurations. The term ΔC_D is the difference between C_D at a given lift coefficient and C_{D_0} for a symmetrical wing configuration; therefore the increment in drag-due to-lift of a cambered wing is that increment in drag above the zero-lift drag coefficient of a symmetrical wing.

Figure 14 indicates that the drag-due-to-lift factor for the cambered wing configuration is 65 to 75 percent of the symmetrical values at lift coefficient of 0.2 and 75 to 85 percent of symmetrical values at $C_L = 0.35$ for Mach numbers below the drag rise. Figure 15 shows the

variation of drag-due-to-lift factor with Mach number for the two configurations along with $1/C_{L_\alpha}$ and $1/\pi A$ (theoretical limits assuming, respectively, zero and 100 percent leading-edge suction). As can be seen, the cambered wing develops a greater portion of the theoretical predicted leading-edge suction than does the symmetrical wing. Although this comparison should be viewed with caution, it is an interesting if somewhat rough measure of the effect of camber on the drag-due-to-lift of the YF-102 airplane.

The comparison shown in figure 16 indicates that the maximum lift-drag ratio for the cambered configuration is about 20 percent higher than for the symmetrical values throughout the comparable Mach number range. The maximum lift-drag ratio values at $M \approx 0.8$ are about 10.6 and 9.0 for the cambered and symmetrical configurations, respectively.

FLIGHT-TUNNEL COMPARISONS

Comparison has been made of the flight data and unpublished 1/20-scale model data from the Langley 8-foot transonic tunnel. The tunnel data represent Reynolds number values from 3.6×10^6 to 4.6×10^6 based on the mean aerodynamic chord.

Average center-of-gravity positions for flight data and tunnel data were about 29 percent mean aerodynamic chord and 27.5 percent mean aerodynamic chord, respectively. For the comparison, tunnel data were adjusted to the same trim conditions as the flight data by using the elevon deflections shown in figure 9.

Figure 17 shows a comparison of the lift-curve slope variations with Mach number for the flight and tunnel data for both configurations. These data represent the average values for lift coefficients less than 0.3. The cambered wing data show similar trends throughout the Mach number range for both sources. However, for the symmetrical wing data the flight lift-curve slope increases gradually while the tunnel data remain constant as Mach number increases to 0.9. The tunnel data then increase abruptly, continuing for the remainder of the Mach number range near the flight lift-curve slope level. Figure 17(a) presents the ratio of lift-curve slopes for the cambered wing and symmetrical wing configurations.

In figure 18 extrapolated values of flight zero-lift drag coefficient are compared with tunnel data for both configurations. Flight values for the cambered wing are about 75 to 85 percent of the tunnel level prior to the drag rise, and for the symmetrical wing are 80 to 90 percent of the tunnel values. Included in figure 18 is an estimate

of the transonic and supersonic level of C_{D_0} for the model fuselage base exactly proportional to full scale, using the method of reference 4. The drag-rise Mach number, 0.93 for both configurations as predicted by the tunnel tests, agrees with flight data.

The effect of camber on drag-due-to-lift for both flight and tunnel can be seen in figures 19 and 20 where drag coefficient is related to lift coefficient and lift coefficient squared for representative constant Mach numbers.

The comparisons of the maximum lift-drag ratio variation with Mach number shown in figure 21 indicate closer agreement between flight and tunnel for the cambered configuration than for the symmetrical configuration. The symmetrical wing comparison shows about 15 percent difference at $M \approx 0.9$ between flight and tunnel data, whereas at the same Mach number the cambered comparison indicates a 5-percent difference between the data sources. Figure 21(a) presents the ratio of $(L/D)_{max}$ values for the cambered wing and symmetrical wing configurations.

In the correlation of flight and wind-tunnel data the question of Reynolds number effects arises. However, caution must be exercised in attributing differences between flight and wind-tunnel data to Reynolds number effects because the differences lie almost within the accuracy of the data and the models almost always incorporate some compromises and deviations from true scale. The most common deviations result from sting mounting difficulties and the simulation of internal flow, and almost as frequent are deviations resulting from engineering changes made between the time the model tests are run and the time the flight airplane is completed. In the case of the YF-102 airplane, there were three sets of wind-tunnel data covering adequate lift and Mach number ranges. One was from the Langley 8-foot transonic wind tunnel using a model of an earlier configuration having a fuselage 4.2 percent smaller in diameter and a shorter fuselage than a true scale model. The fuselage base had been enlarged to accommodate the sting, but because of the shortened base the boattail angle was approximately correct. For the symmetrical wing configuration the model also had a shortened fuselage nose.

The other sets of data are from the Wright Air Developement Center 10-foot transonic wind tunnel and the Southern California Cooperative Wind Tunnel, Pasadena, Calif. These two sets of data used the same model for which the fuselage nose and center section were true to scale, but the fuselage rear section was too long. The data were not used for comparison purposes because there was no air flow through the model and the inlet ducts were faired into the forward part of the fuselage. For flight in the transonic speed region, inlet mass flow ratios range in the vicinity of 90 percent, so the free-stream area of the internal air amounts to 9.9 percent of the fuselage cross-sectional area. The serious

consequences of the lack of simulation of the internal air flow are presented in references 5 and 6. The latter reference indicates drag errors in the transonic region amounting to as much as 20 percent and more, resulting from closing and fairing the inlets. Consequently, it was felt that the deviations from true scale were less significant for the Langley 8-foot tunnel models and data from these models were used in this paper for comparison.

The WADC 10-foot transonic wind-tunnel data give an indication of Reynolds number effects because, with the same model, Reynolds numbers based on the mean aerodynamic chord of 2.2×10^6 and 4.8×10^6 were obtained by varying the tunnel air density. Figure 22 presents data for the cambered wing configuration at a Mach number of 0.8 and zero lift for the WADC tests, the Langley 8-foot transonic tunnel tests, and flight tests. Also shown in this figure is a curve of turbulent flow skin friction taken from the theoretical work of Van Driest (ref. 7), and corrected from a surface area basis to a wing area basis by multiplying by 2.72, the ratio of surface area to wing area. It is interesting to note in figure 22 that the two WADC test points and also the 8-foot tunnel test point combined with the flight data show decreases in drag with increasing Reynolds number, comparable to that of the Van Driest theoretical skin-friction curve. However, it is felt that because of the accuracies of the flight and tunnel data presented in this paper, because of deviation of the models from true scale, and because none of the models simulated the engine jet, which references 5 and 6 regard as important, no quantitative statement concerning Reynolds number effects can be made from the flight data.

SUMMARY OF RESULTS

Flight evaluation of the lift and drag characteristics of the Convair YF-102 airplane with both symmetrical and cambered wing configurations gave the following results:

1. The lift-curve slopes increased gradually over the lift-coefficient range from 0.1 to 0.4 with greater increase for the symmetrical wing configuration than for the cambered wing configuration.

2. The modifications comprising the cambered wing configuration caused an increase in the angle of attack for zero lift of less than 0.5° over the Mach number range.

3. The cambered wing configuration had lower drag-coefficient values for lift coefficients above 0.1, with maximum decrease in drag coefficient of about 0.01 occurring at a lift coefficient of about 0.3.

4. At lift-coefficient values of about 0.2 the drag-due-to-lift for the cambered wing configuration is 65 to 75 percent of the symmetrical wing configuration for Mach numbers below the drag rise. At a lift coefficient of 0.35 the drag-due-to-lift for the cambered wing is from 75 to 85 percent of the symmetrical wing configuration.

5. The maximum lift-drag ratio for the cambered wing is almost 20 percent higher than for the comparable symmetrical wing values throughout the Mach number range.

6. Comparisons of flight and tunnel drag characteristics suggest a tendency of zero-lift drag coefficient to decrease with increasing Reynolds number; however, it cannot be determined from these comparisons what part of the zero-lift drag coefficient change is due to Reynolds number and what portion should be attributed to model variations from exact reproductions, or to inaccuracies in the data.

High-Speed Flight Station,
National Advisory Committee for Aeronautics,
Edwards, Calif., April 23, 1956.

REFERENCES

1. Rogallo, Vernon L.: Effects of Wing Sweep on the Upwash at the Propeller Planes of Multiengine Airplanes. NACA TN 2795, 1952.

2. Yaggy, Paul F.: A Method for Predicting the Upwash Angles Induced at the Propeller Plane of a Combination of Bodies With an Unswept Wing. NACA TN 2528, 1951.

3. Brunn, Cyril D., and Stillwell, Wendell H.: Mach Number Measurements and Calibrations During Flight at High Speeds and at High Altitudes Including Data for the D-558-II Research Airplane. NACA RM H55J18, 1956.

4. Nelson, Robert L., and Stoney, William E., Jr.: Pressure Drag of Bodies at Mach Numbers Up to 2.0. NACA RM L53I22c, 1953.

5. Seddon, J., and Nicholson, L. F.: The Representation of Engine Airflow in Wind Tunnel Model Testing. Tech. Note No. Aero 2371, British R.A.E., May 1955.

6. Evans, Albert J.: The Simulation of the Effects of Internal Flow in Wind Tunnel Model Tests of Turbo-Jet Powered Aircraft. Presented to Wind Tunnel Model and Model Testing Panel of Advisory Group for Aeronautical Research and Development, Ottawa, Canada, June 10 to 14, 1955.

7. Van Driest, E. R.: Turbulent Boundary Layer in Compressible Fluids, vol. 18, no. 3, Jour. Aero. Sci., March 1951, pp. 145-160.

TABLE I

PHYSICAL CHARACTERISTICS OF THE TEST AIRPLANE

	Cambered	Symmetrical
Wing:		
Airfoil section	NACA 0004-65 (modified)	NACA 0004-65 (modified)
Total area, sq ft	695.05	661.50
Span, ft	38.11	37.03
Mean aerodynamic chord, ft	23.76	23.13
Root chord, ft	35.63	34.69
Tip chord, ft	0.81	0
Taper ratio	0.023	0
Aspect ratio	2.08	2.20
Sweep at leading edge, deg	60.1	60
Incidence, deg	0	0
Dihedral, deg	0	0
Conical camber (leading edge), percent chord	6.3	None
Geometric twist, deg	0	0
Inboard fence, percent wing span	37	None
Outboard fence, percent wing span	67	67
Tip reflex, deg	10	0
Maximum thickness:		
Root, percent chord	3.9	4.0
Outboard edge of elevon, percent chord	3.5	4.0
Elevons:		
Area (total, both rearward of hinge line), sq ft	67.77	67.77
Span (one elevon), ft	13.26	13.26
Root chord (rearward of hinge line) parallel to fuselage center line, ft	3.15	3.15
Tip chord (rearward of hinge line), ft	2.03	2.03
Elevator travel, deg:		
Up	35	35
Down	20	20
Aileron travel total, deg	20	20
Operation	Hydraulic	Hydraulic
Vertical tail:		
Airfoil section	NACA 0004-65 (modified)	
Area (above water line 33.00), sq ft	68.33	
Sweep at leading edge, deg	60	
Height above fuselage center line, ft	11.41	
Rudder:		
Area (rearward of hinge line), sq ft	10.47	
Span, ft	5.63	
Root chord (rearward of hinge line), ft	2.10	
Tip chord (rearward of hinge line), ft	1.61	
Travel, deg	±25	
Operation	Hydraulic	
Fuselage:		
Length, ft	52.4	
Maximum diameter, ft	6.5	
Power plant:		
Pratt and Whitney	J57-P11 turbojet engine with afterburner	
Static thrust at sea level, lb	9,700	
Static thrust at sea level, afterburner, lb	14,800	
Center-of-gravity location, percent $\bar{c}$:		
Empty weight	25.6	
Total weight	29.8	
Moments of inertia (estimated for 24,000-lb gross weight):		
I_X, slug-ft^2	13,200	
I_Y, slug-ft^2	106,000	
I_Z, slug-ft^2	114,600	
I_{XZ}, slug-ft^2	3,540	
Inclination of principal axis (estimated) below reference axis at nose, deg	2	

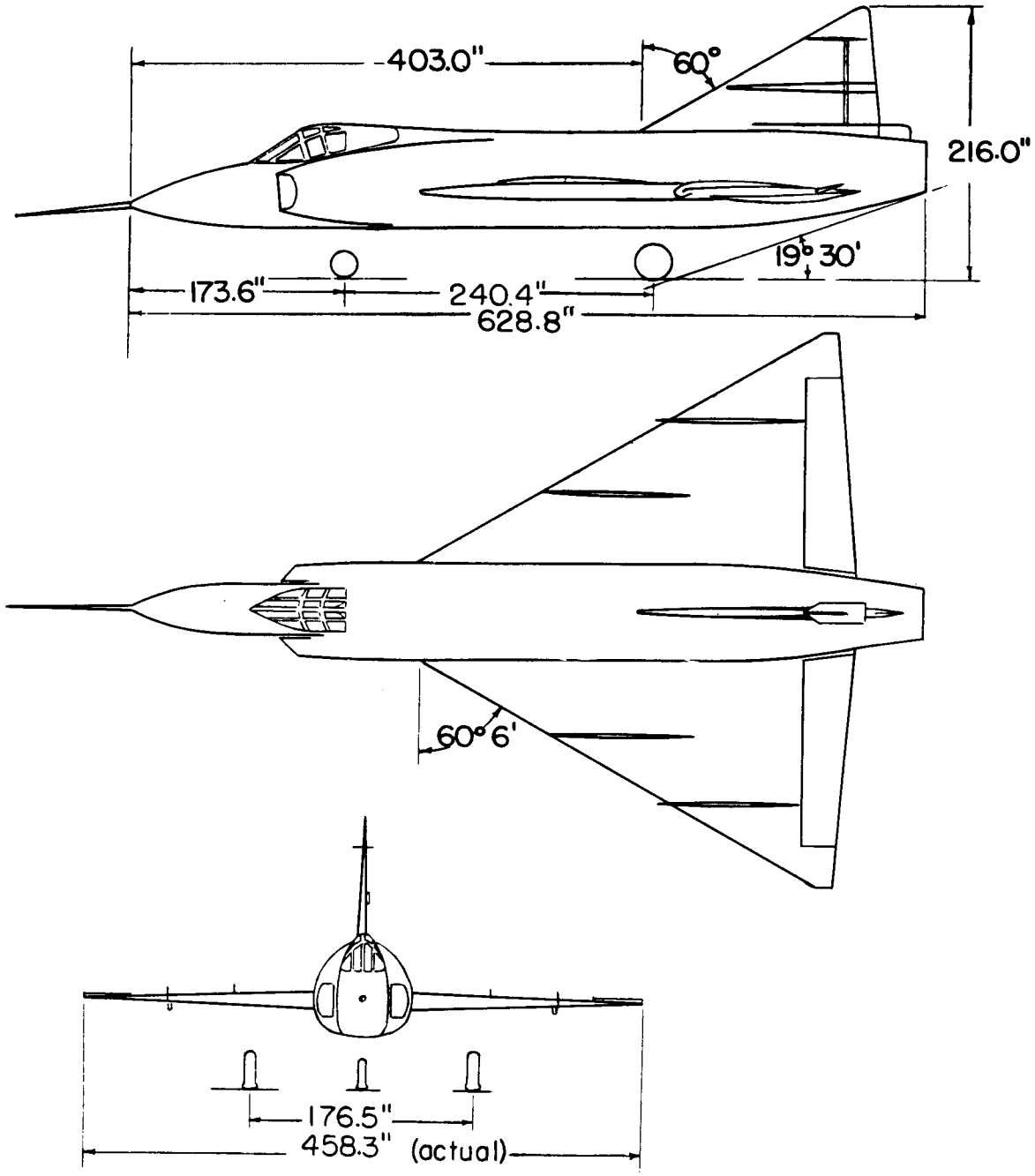

(a) Cambered wing.

Figure 1.- Three-view drawings of the YF-102 airplane.

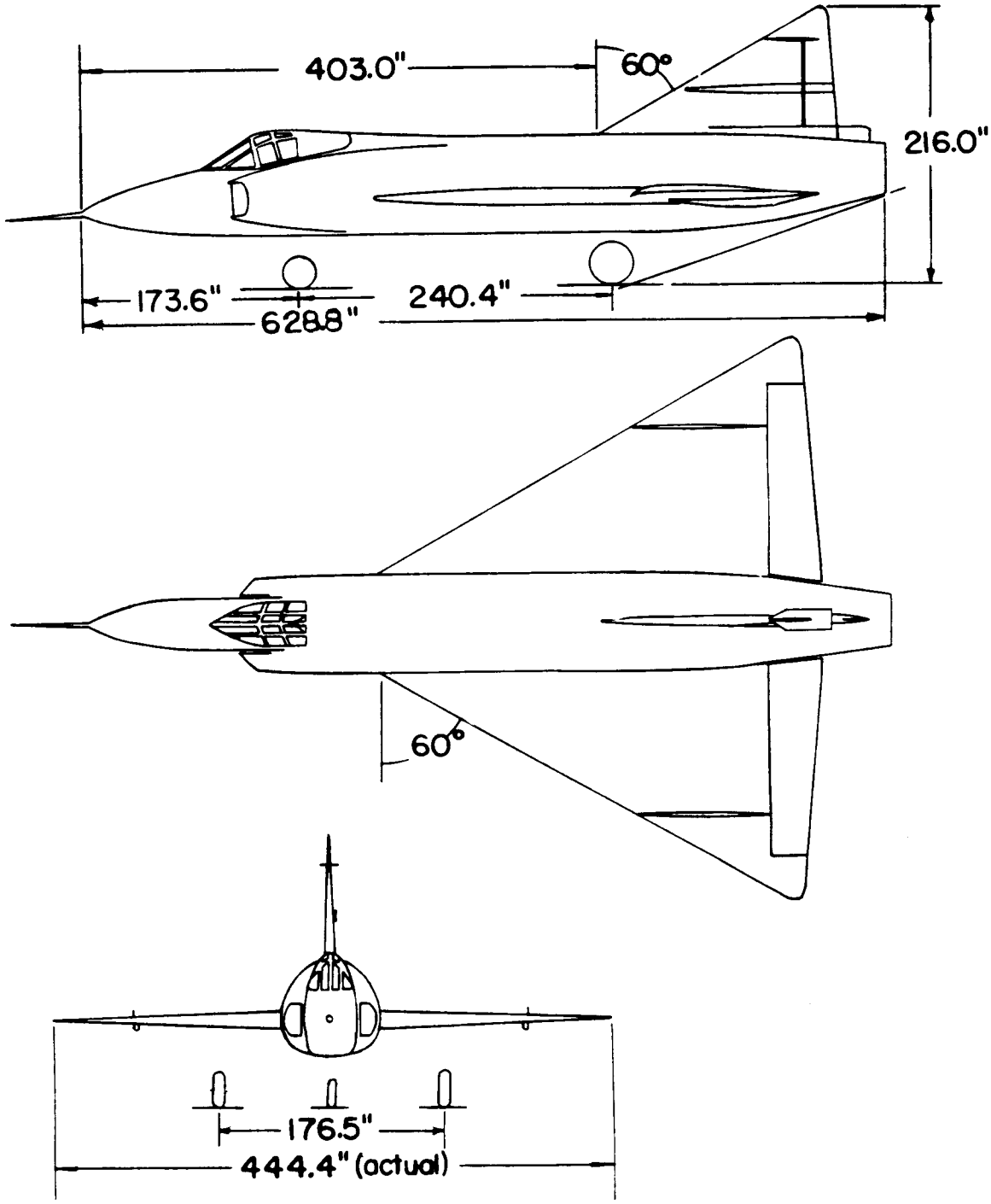

(b) Symmetrical wing.

Figure 1.- Concluded.

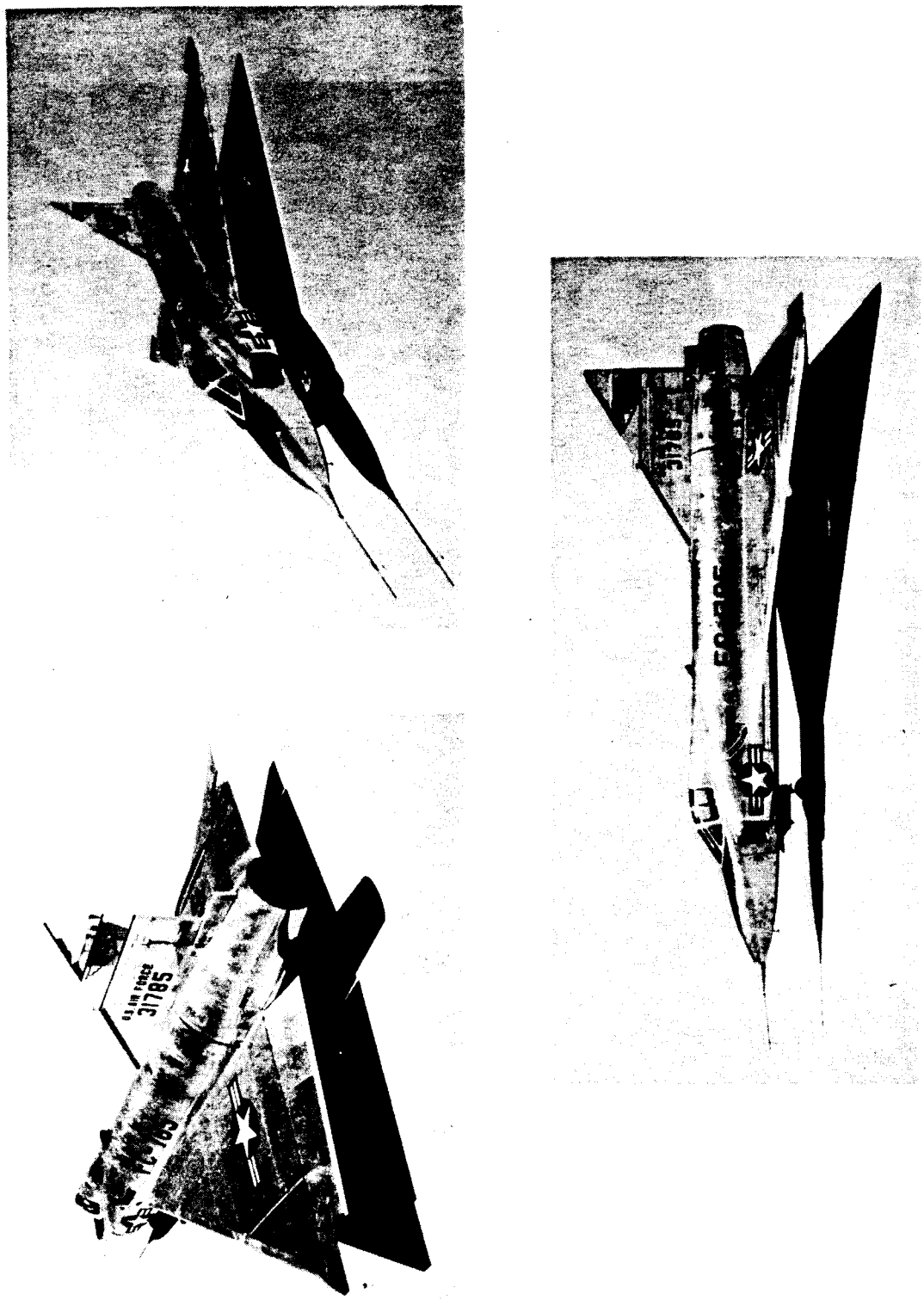

E-1838

Figure 2.- Photographs of the YF-102 airplane with cambered wing.

E-1992

Figure 3.- View of underside of wing of YF-102 airplane showing cambered leading edge.

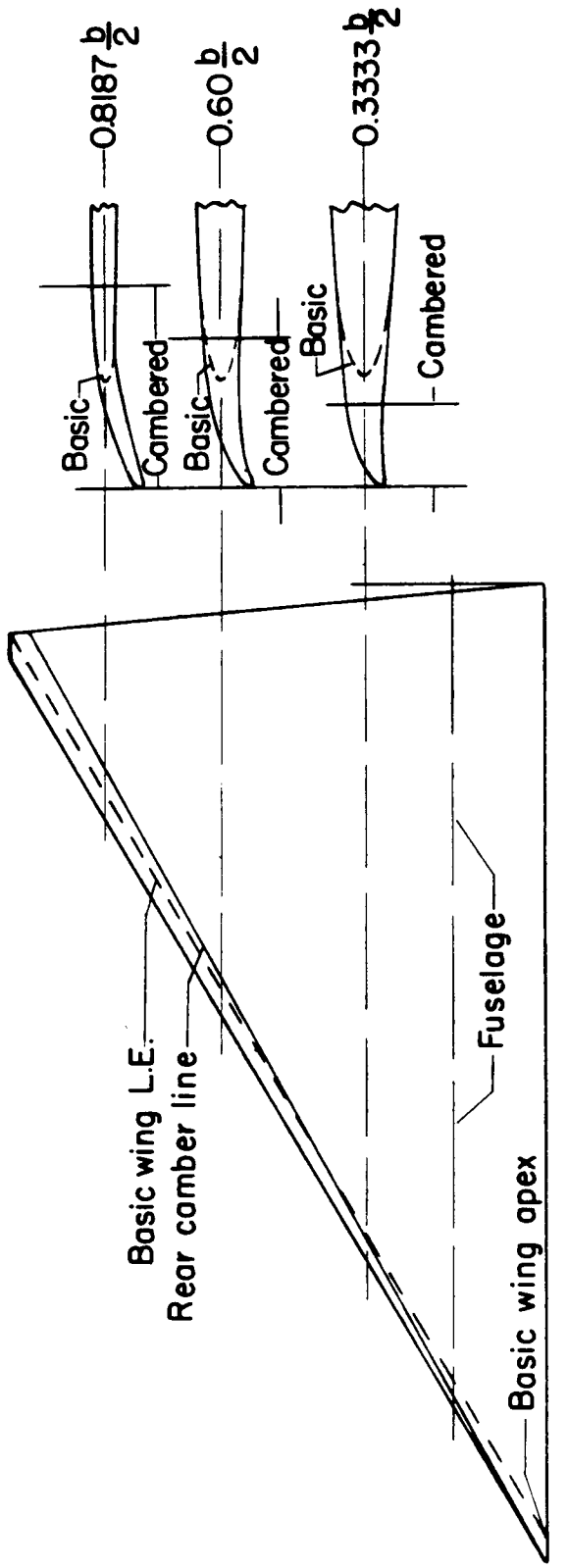

Figure 4.- Details of leading-edge camber.

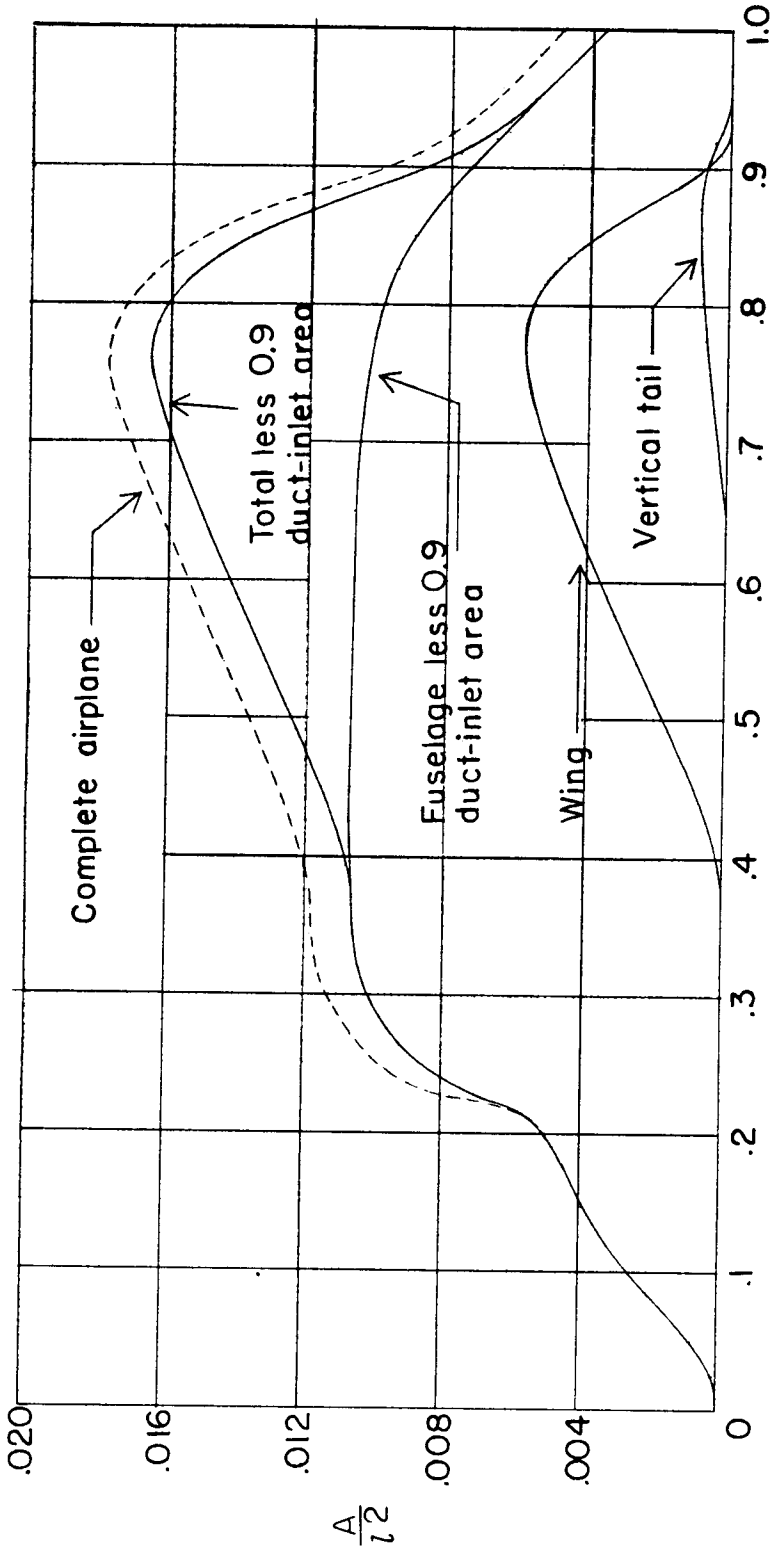

Figure 5.- Cross-sectional area distribution of the YF-102 airplane.

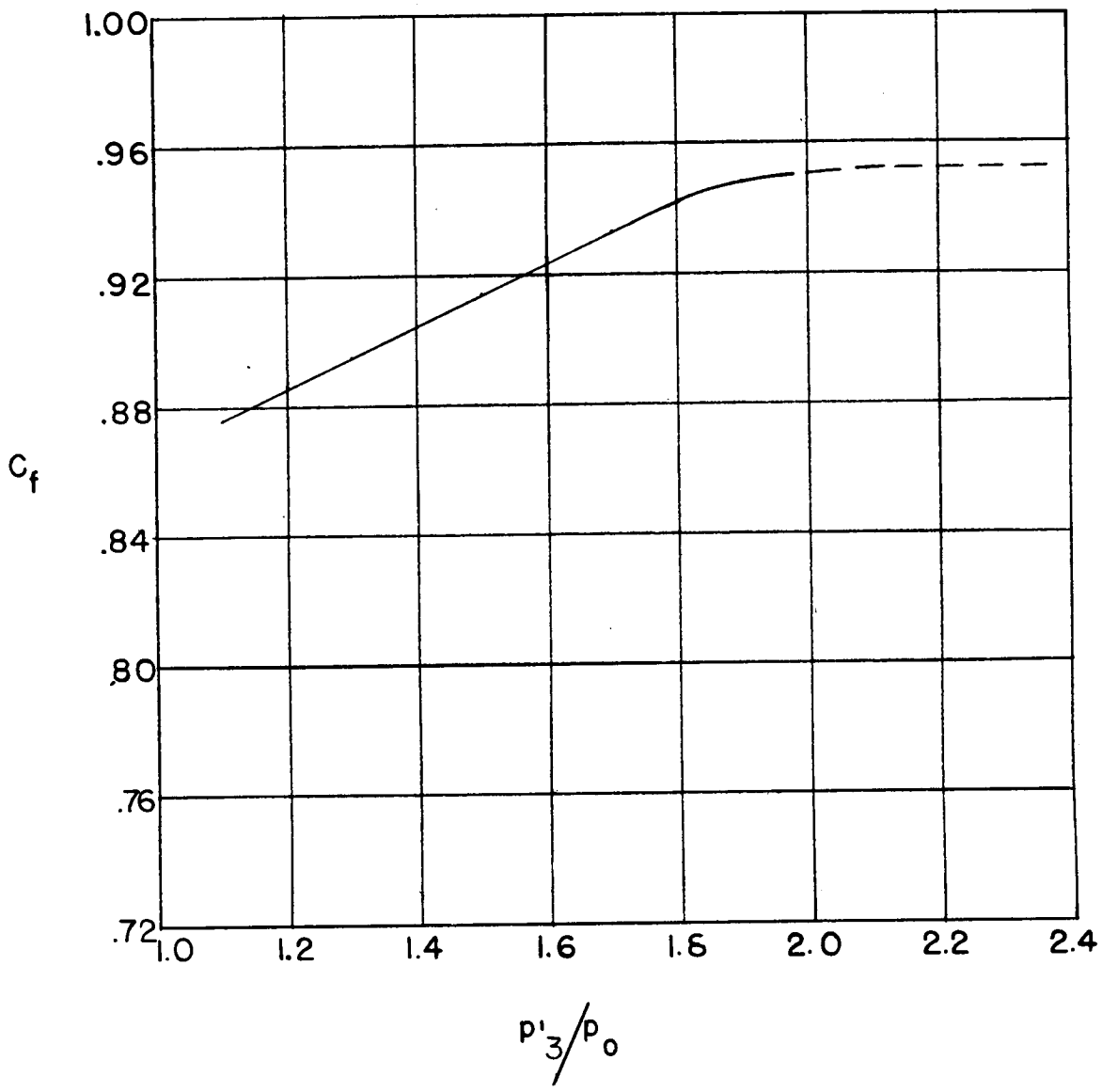

Figure 6.- Variation of thrust coefficient with exit pressure ratio for afterburner-on and afterburner-off conditions.

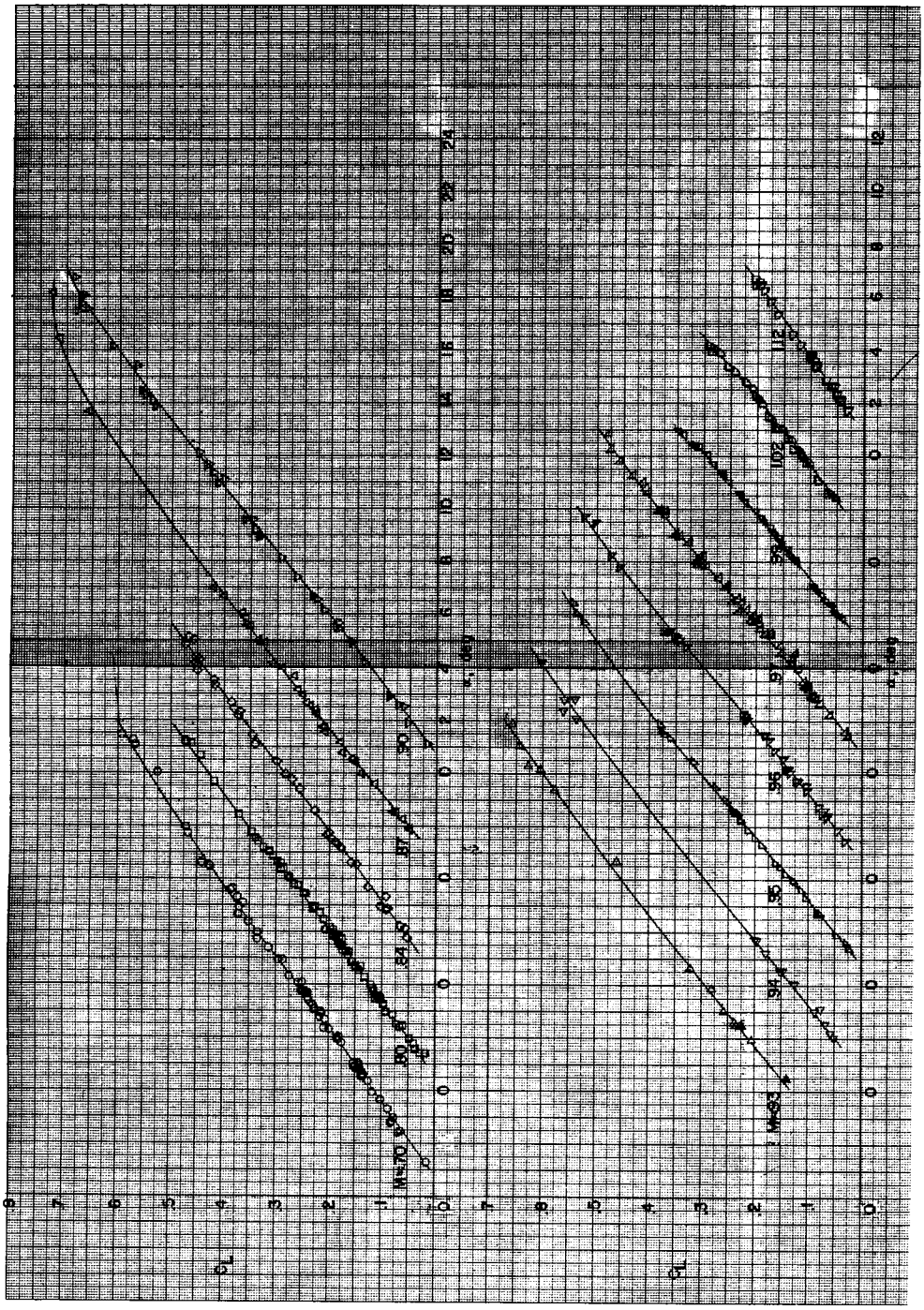

(a) Cambered wing.

Figure 7.- Variation of lift coefficient with angle of attack. Trimmed flight. Solid points indicate data from stabilized level runs.

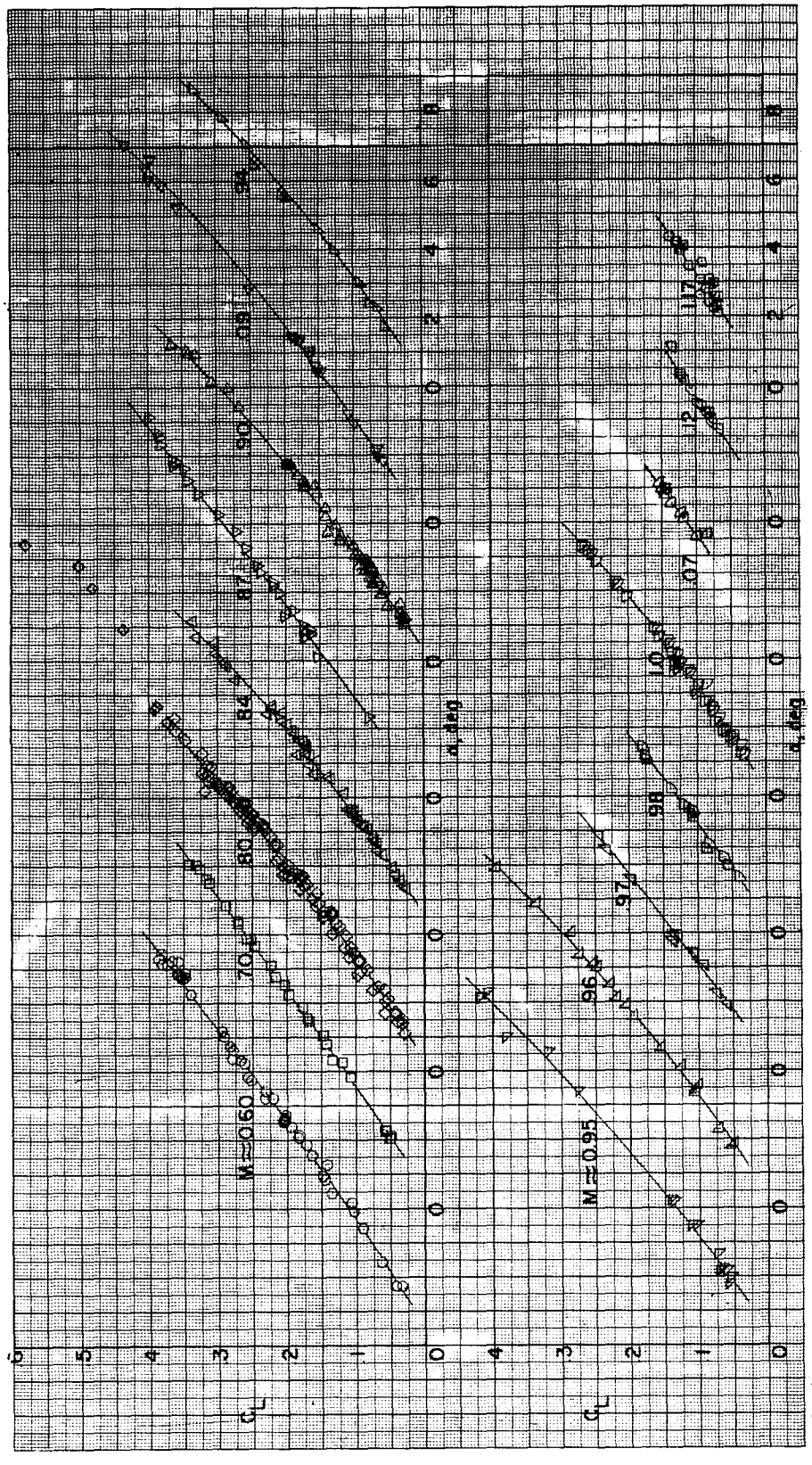

(b) Symmetrical wing.

Figure 7.- Concluded.

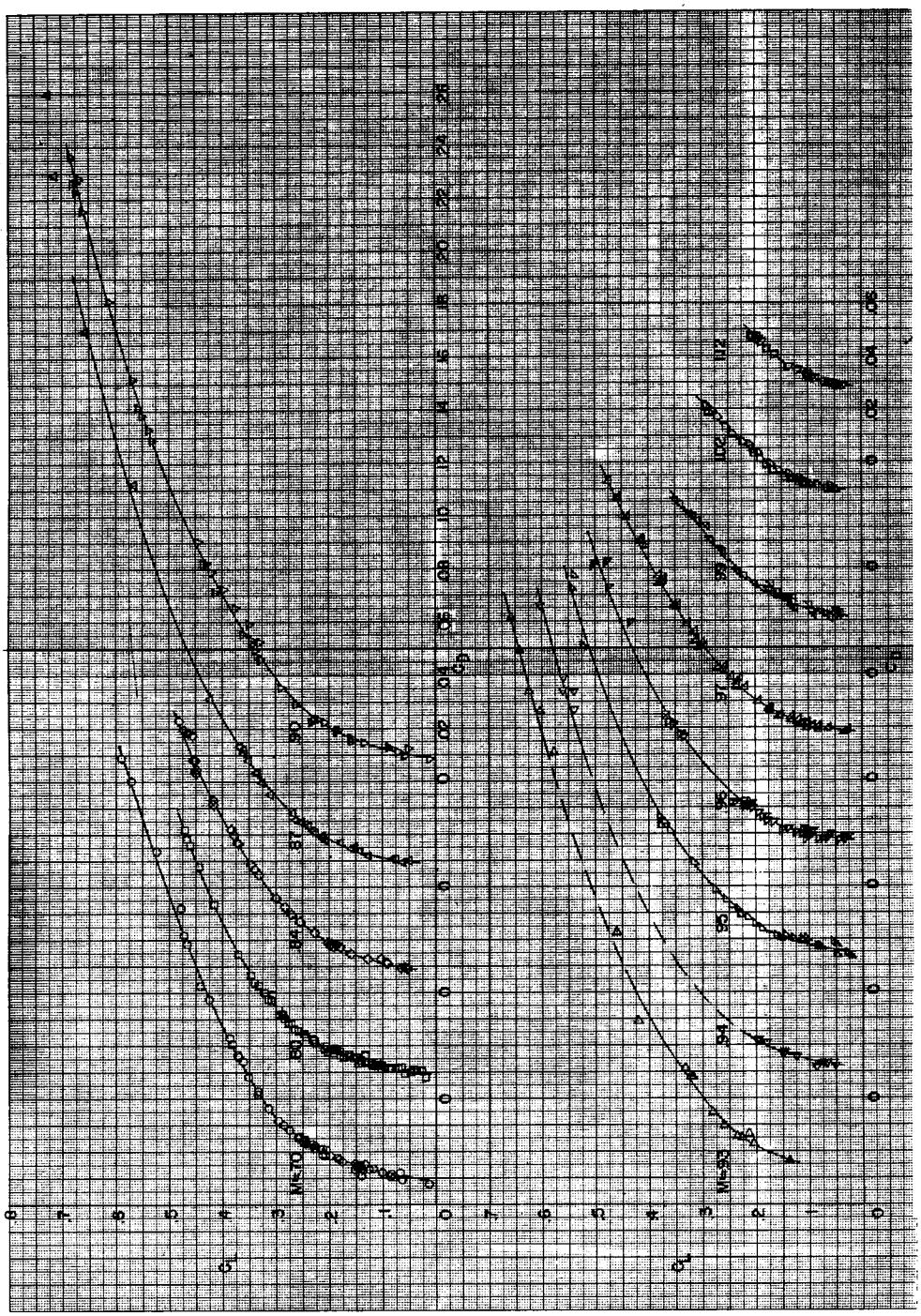

(a) Cambered wing.

Figure 8.- Variation of drag coefficient with lift coefficient. Trimmed flight. Solid points indicate data from stabilized level runs.

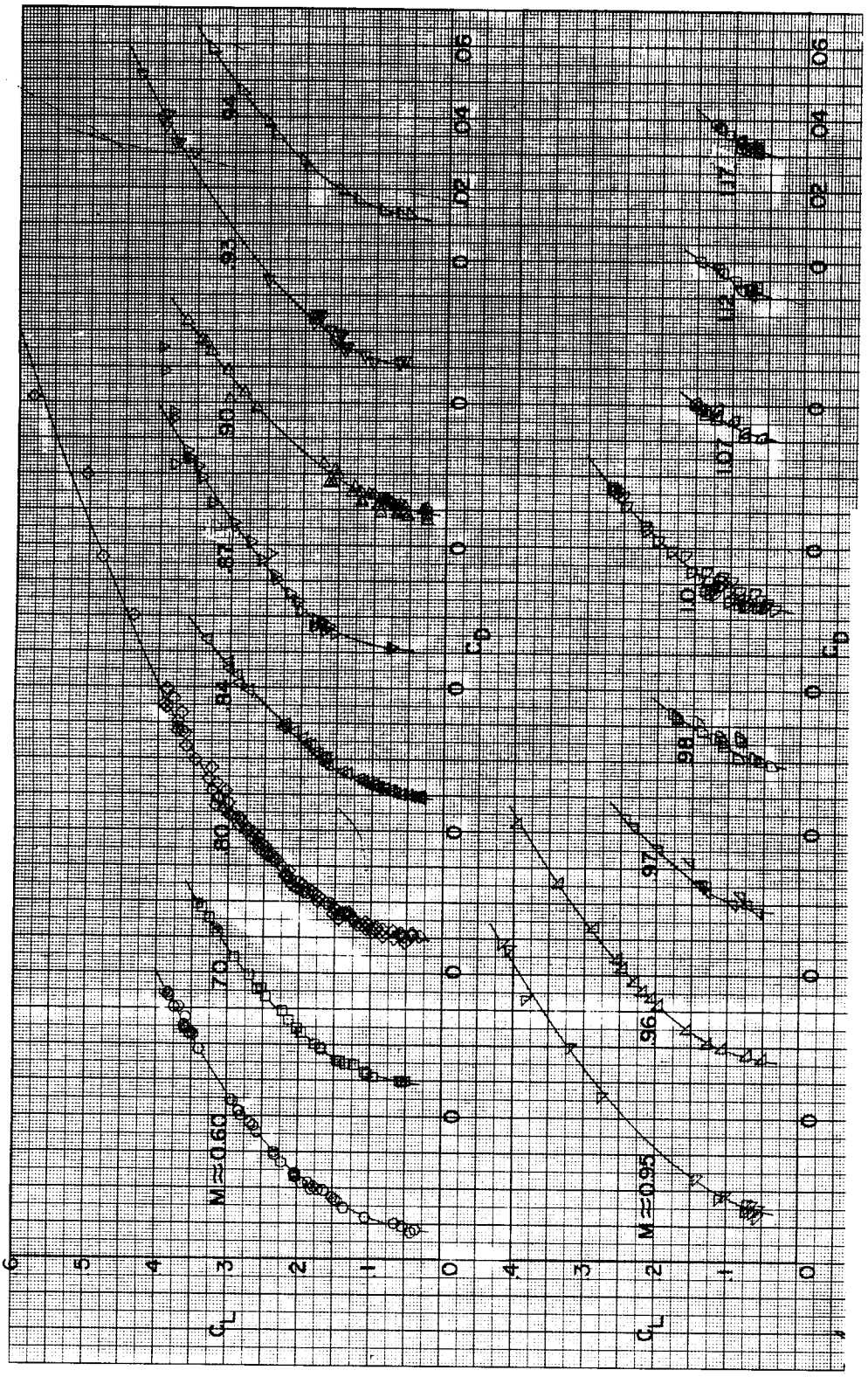

(b) Symmetrical wing.

Figure 8.- Concluded.

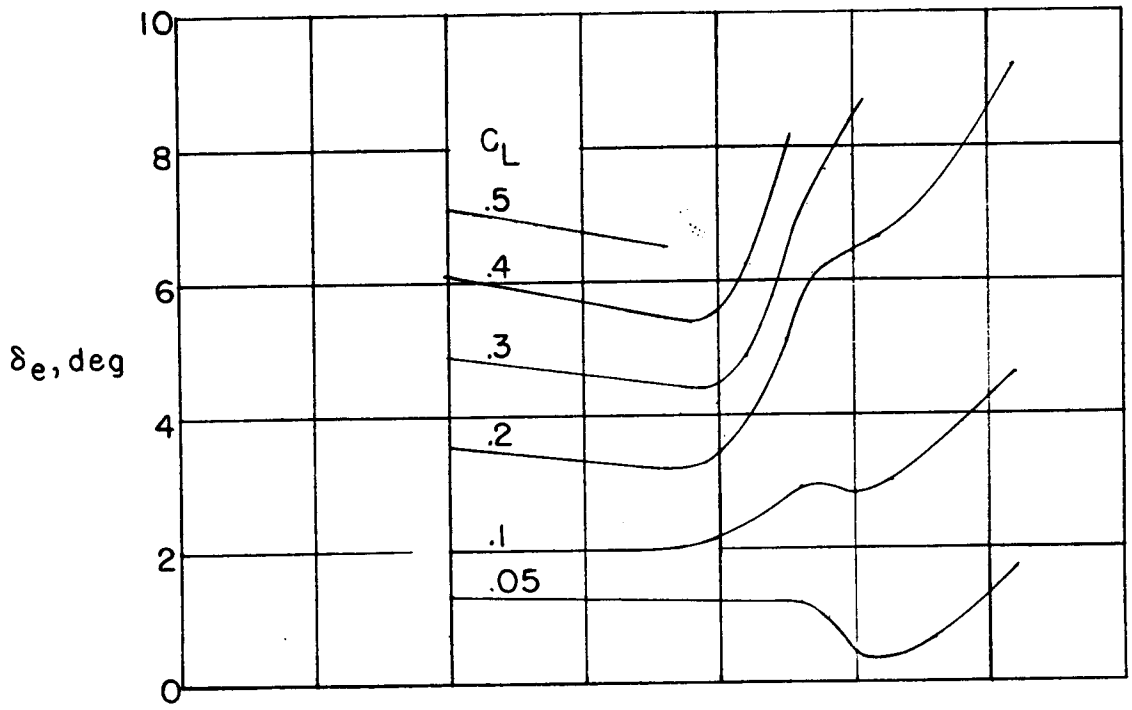

(a) Cambered.

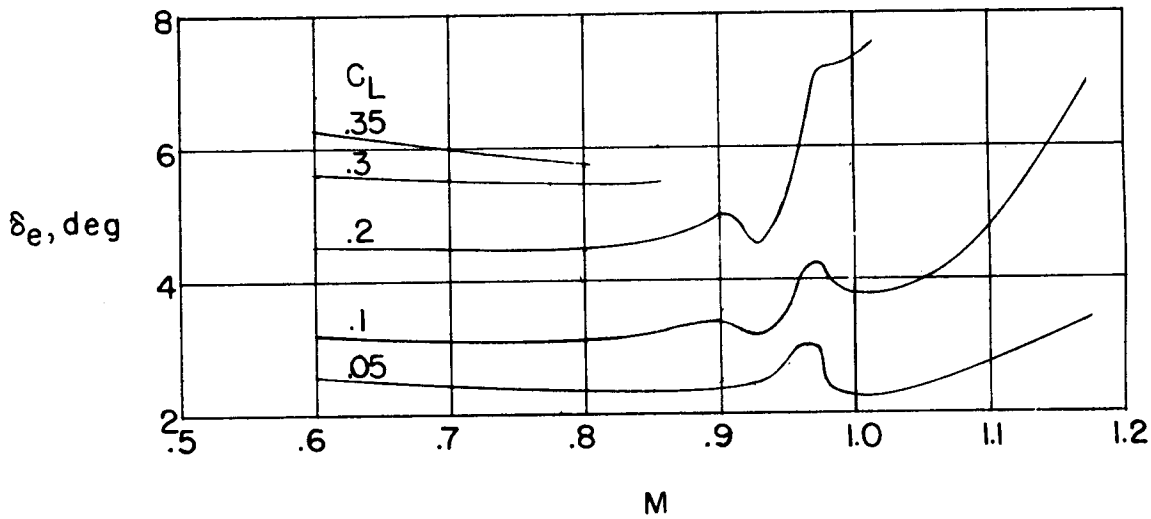

(b) Symmetrical.

Figure 9.- Flight trim characteristics for the YF-102 airplane.

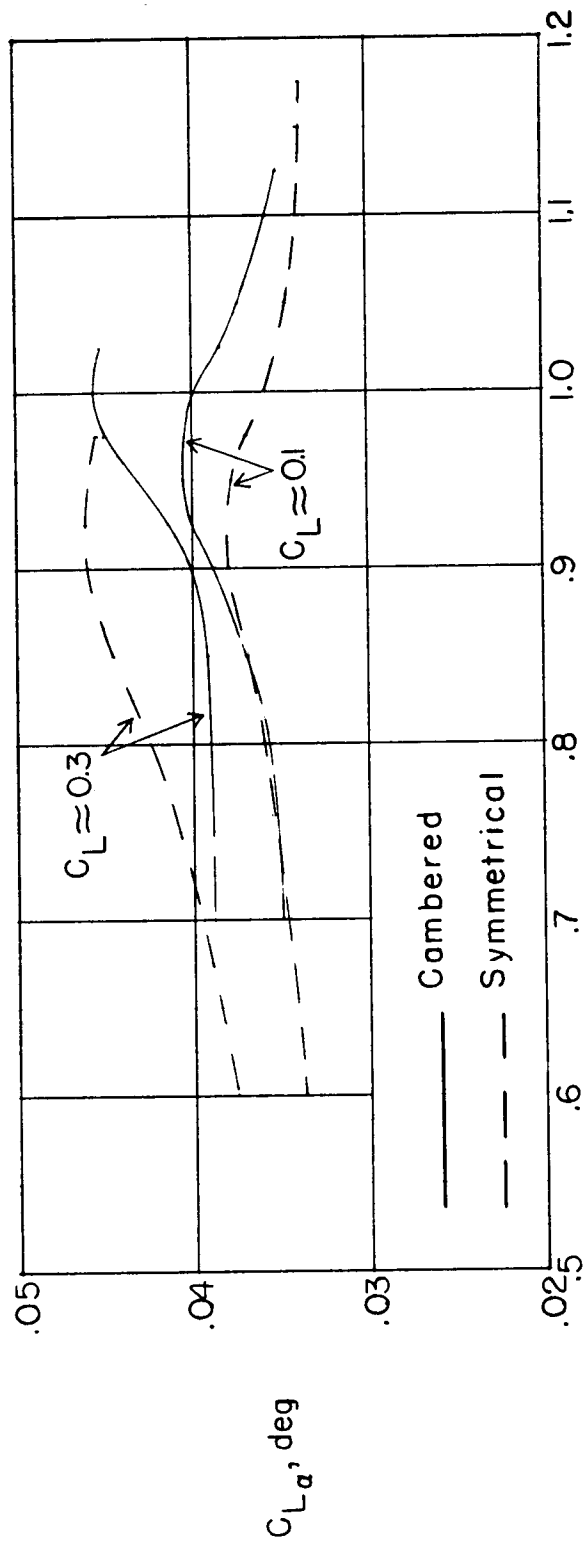

Figure 10.- Comparison of the relationship of lift-curve slope and Mach number. Trimmed flight.

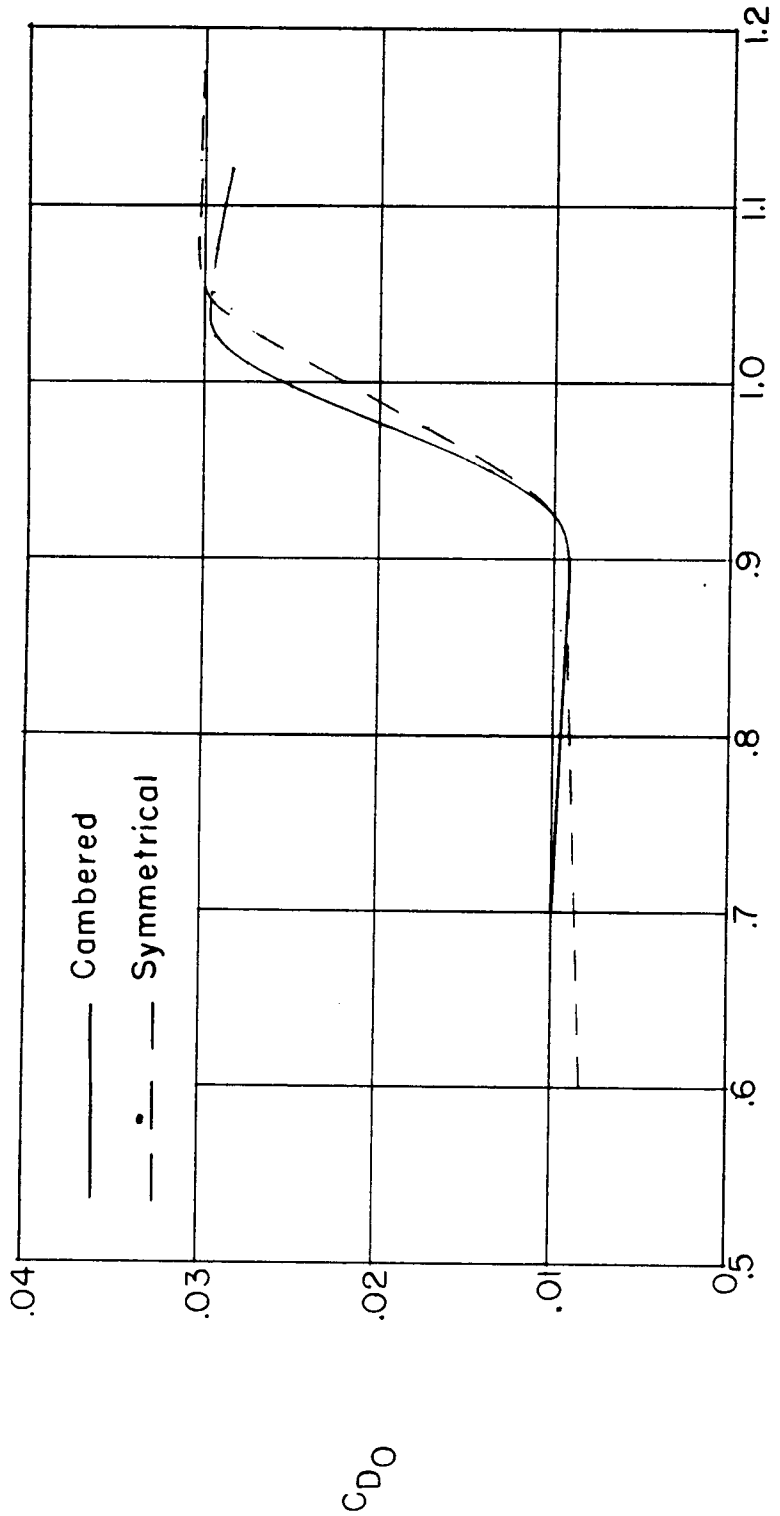

Figure 11.- Comparison of the relationship of zero-lift drag coefficient and Mach number. Trimmed flight.

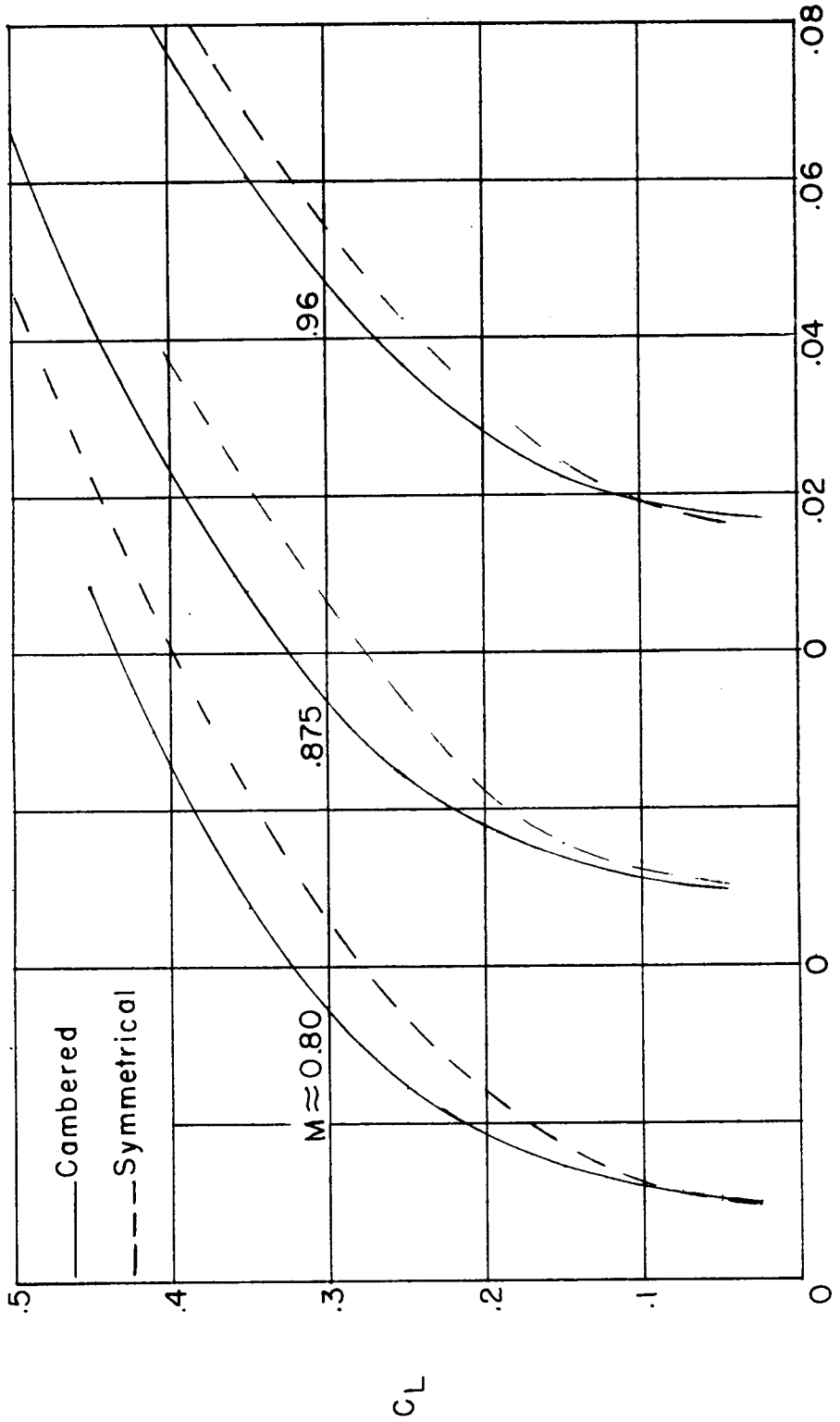

Figure 12.- Comparison of lift-drag relationship at representative Mach numbers. Trimmed flight.

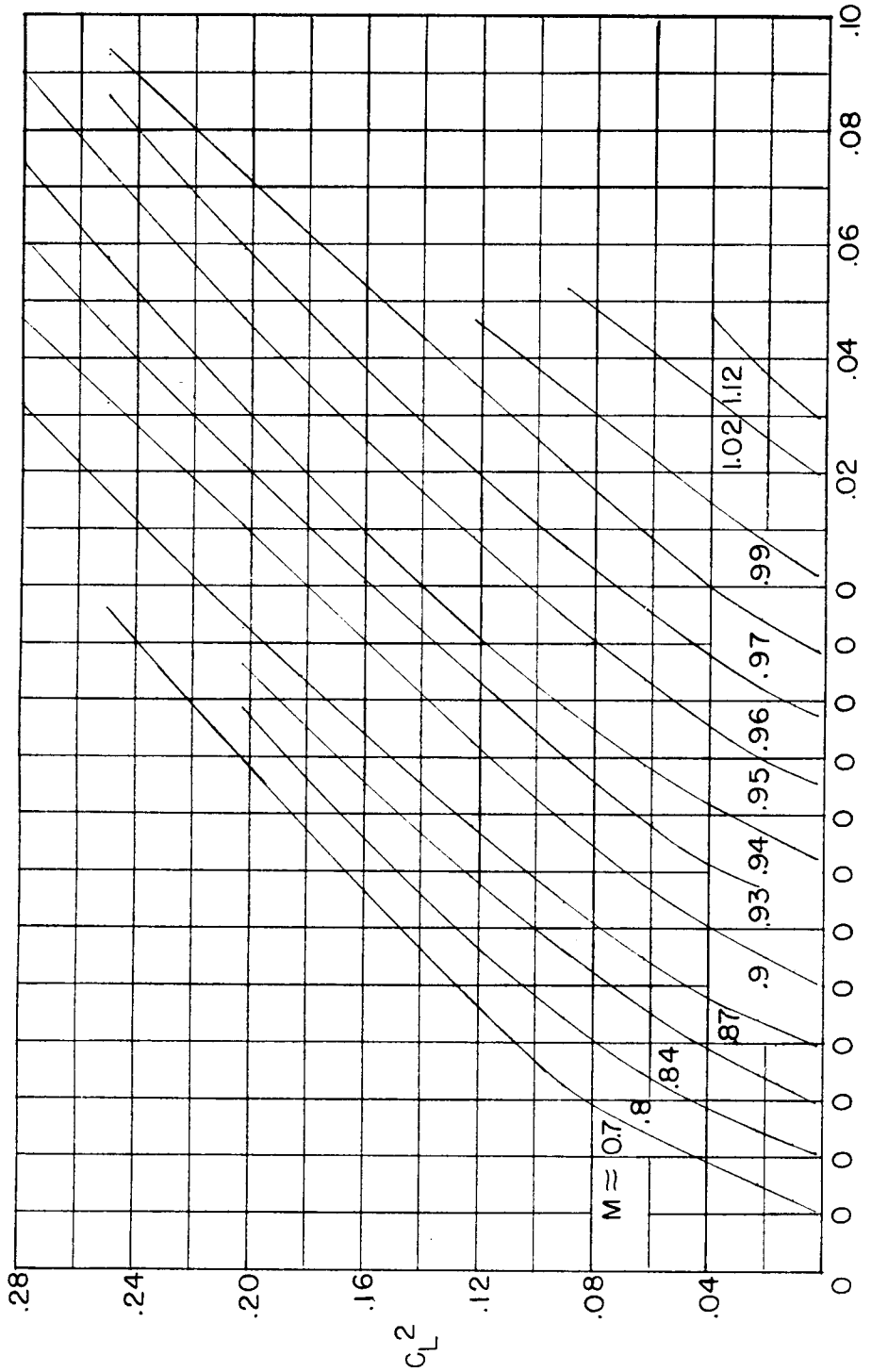

(a) Cambered wing.

Figure 13.- Relationship of lift coefficient squared and drag coefficient for trimmed flight.

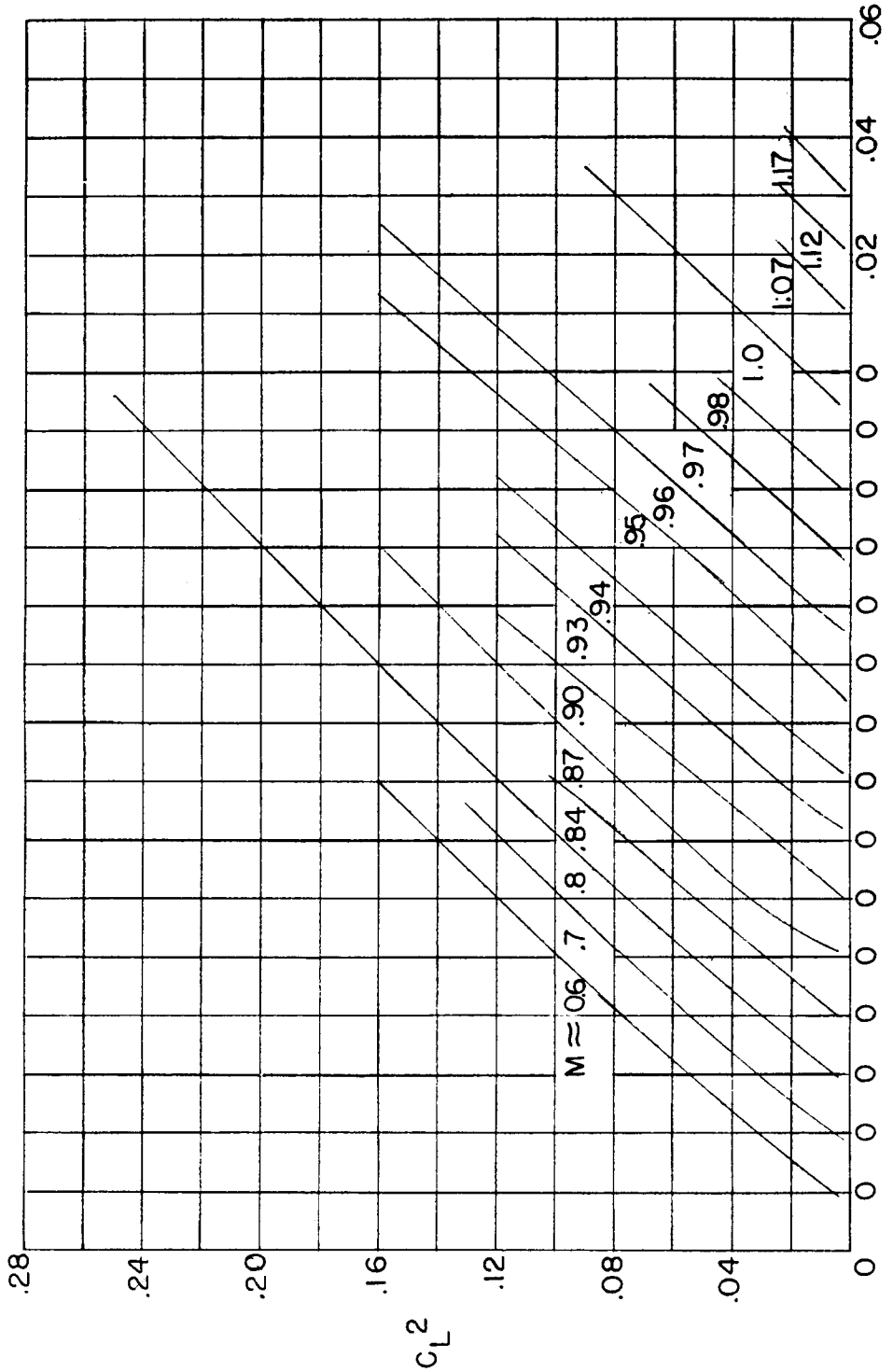

(b) Symmetrical wing.

Figure 13.- Concluded.

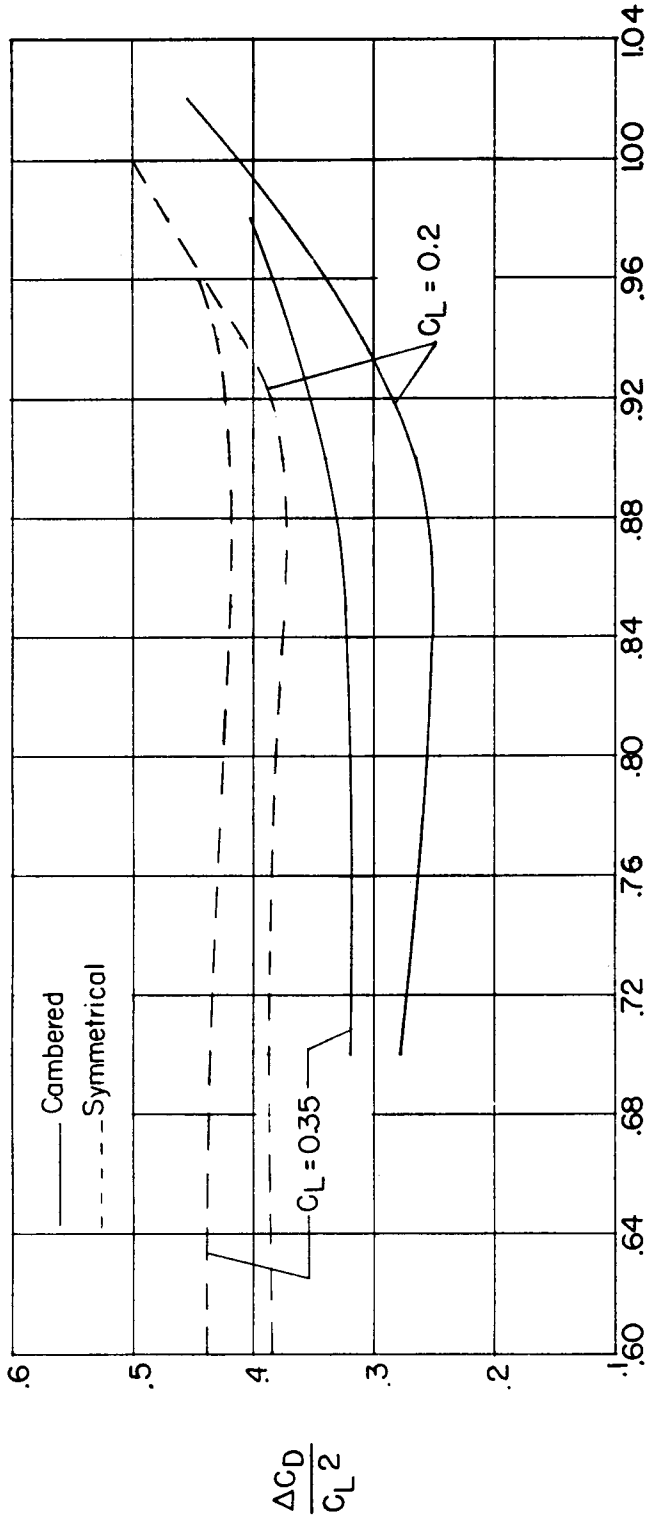

Figure 14.- Comparison of the relationship of drag-due-to-lift factor and Mach number. Trimmed flight.

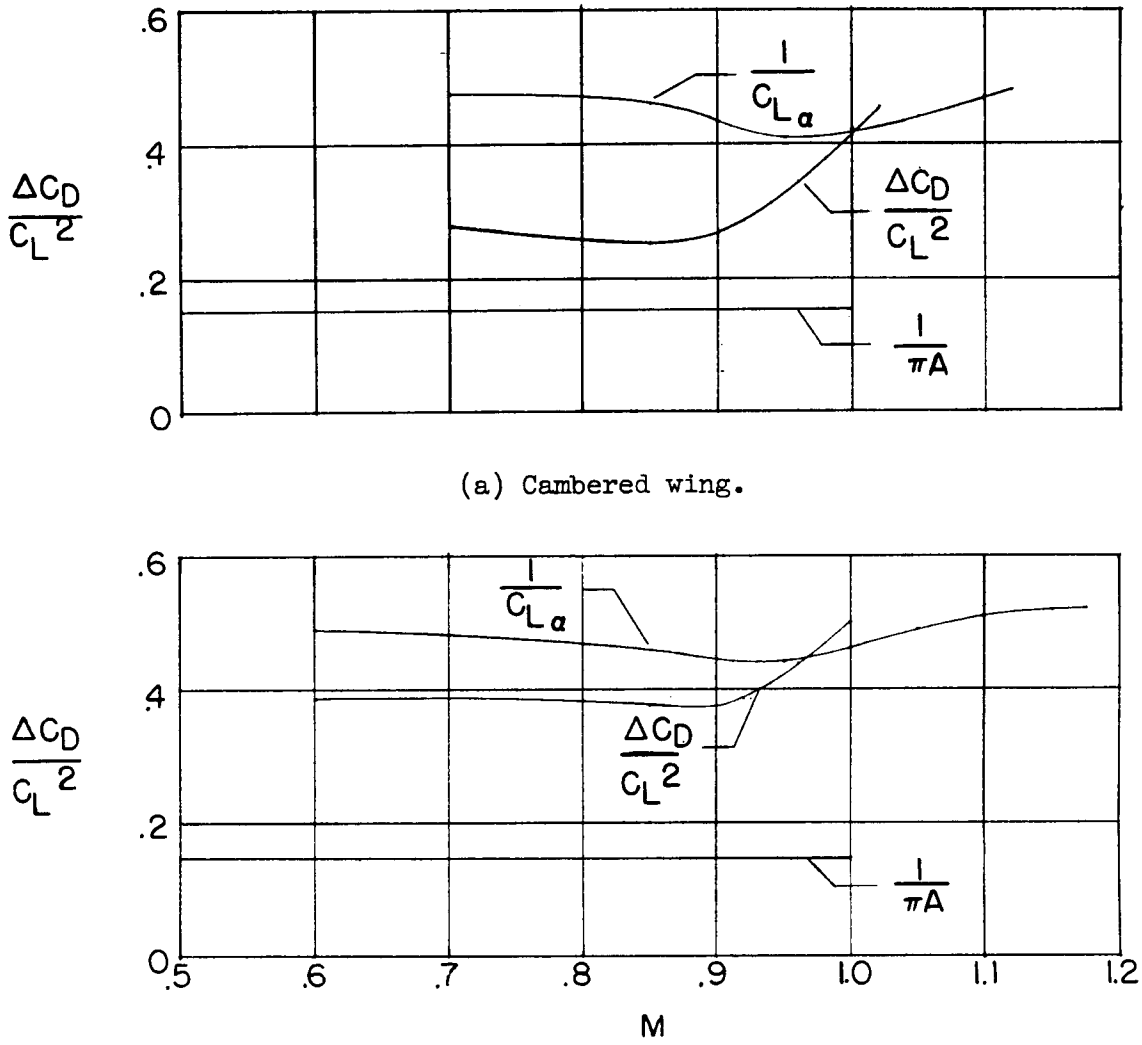

(a) Cambered wing.

(b) Symmetrical wing.

Figure 15.- Comparison of drag-due-to-lift factor with theoretical limits throughout Mach number range. Trimmed flight; $C_L = 0.2$.

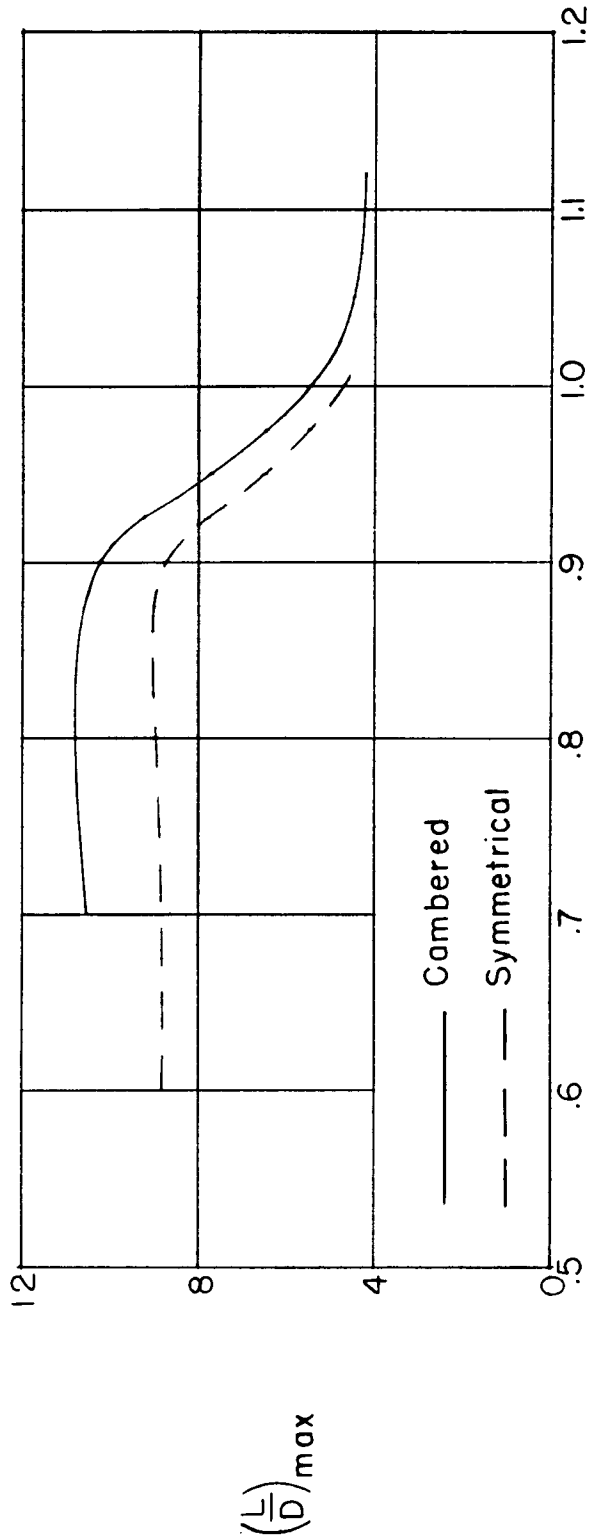

Figure 16.- Comparison of the relationship of maximum lift-drag ratio and Mach number. Trimmed flight.

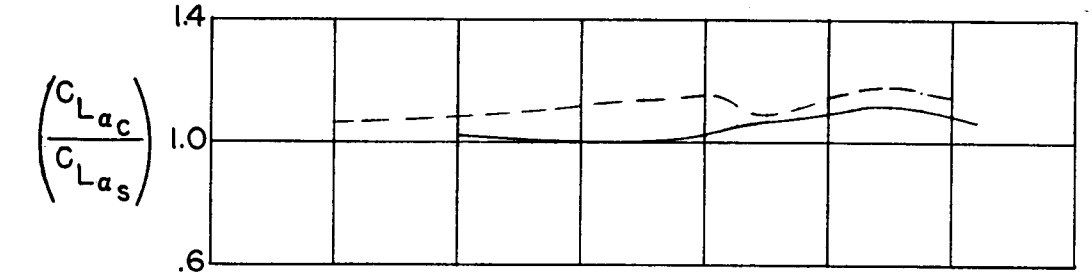

(a) Ratio, cambered to symmetrical.

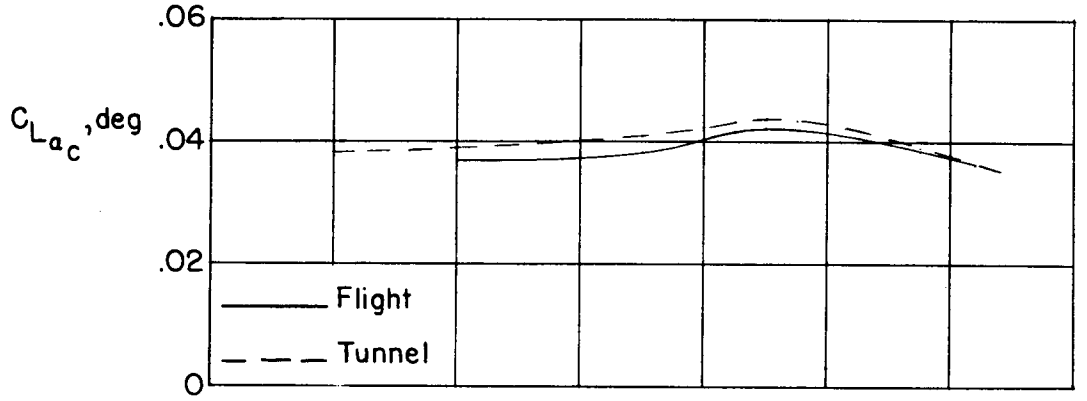

(b) Cambered.

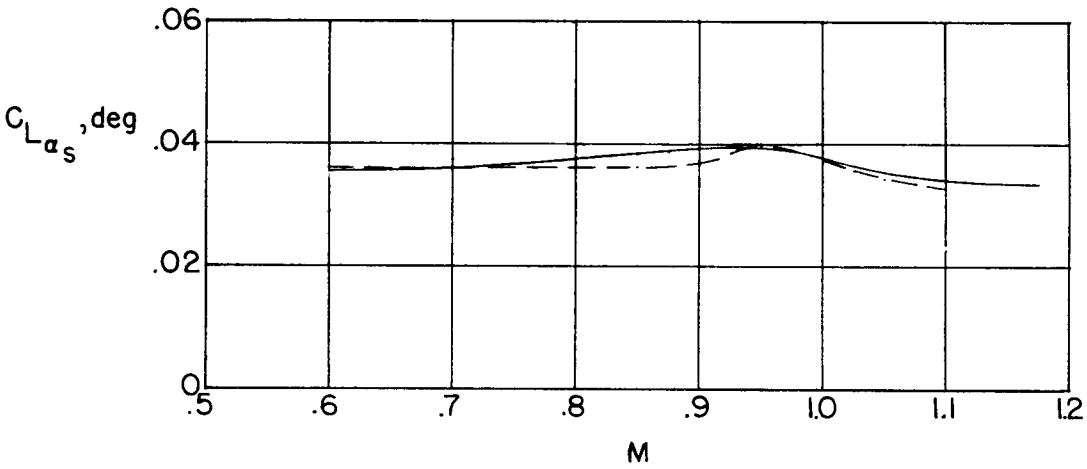

(c) Symmetrical.

Figure 17.- Comparison of lift-curve slope as measured in flight and wind tunnel. Trimmed condition.

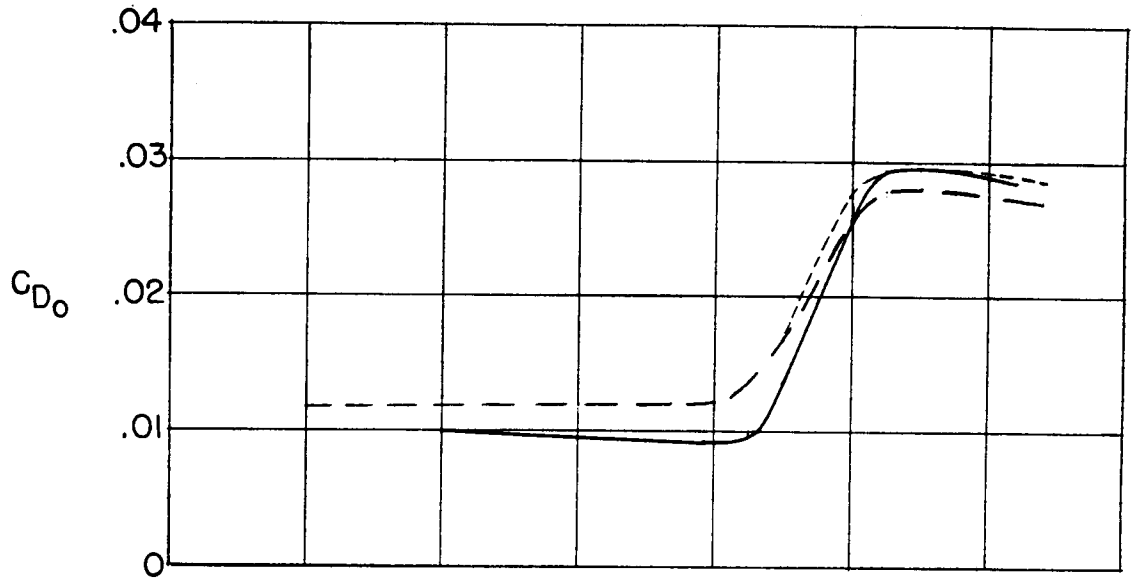

(a) Cambered.

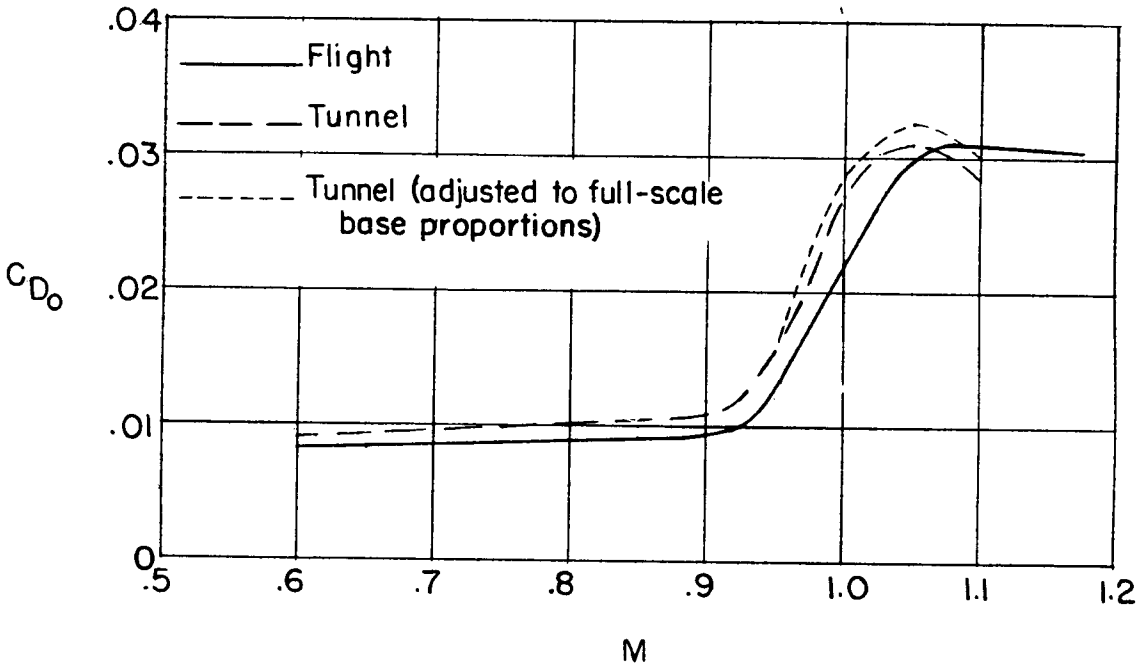

(b) Symmetrical.

Figure 18.- Comparison of zero-lift drag coefficient as measured in flight and wind tunnel. Trimmed condition.

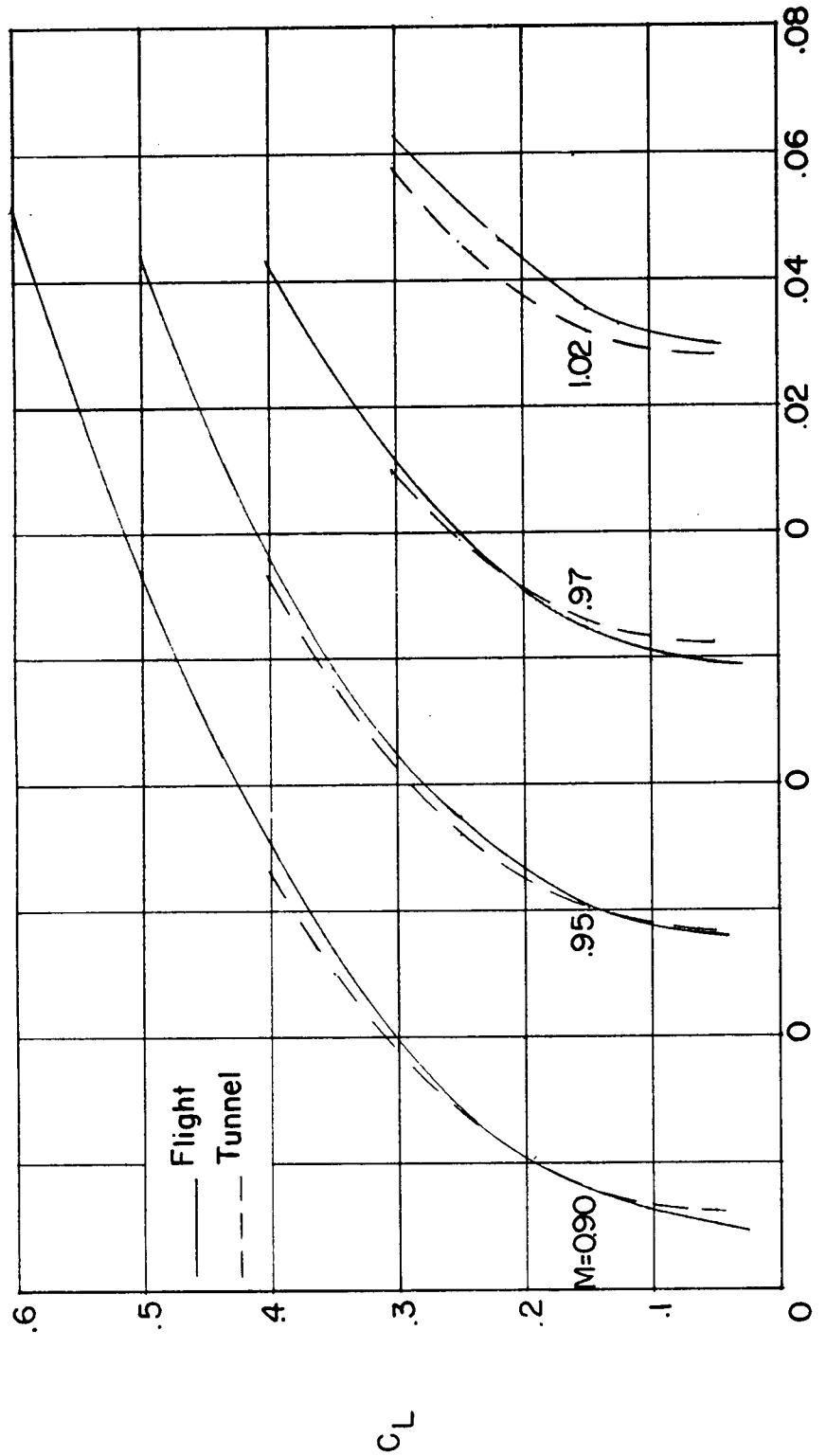

(a) Cambered wing.

Figure 19.- Variation of drag coefficient with lift coefficient for several Mach numbers. Trimmed condition.

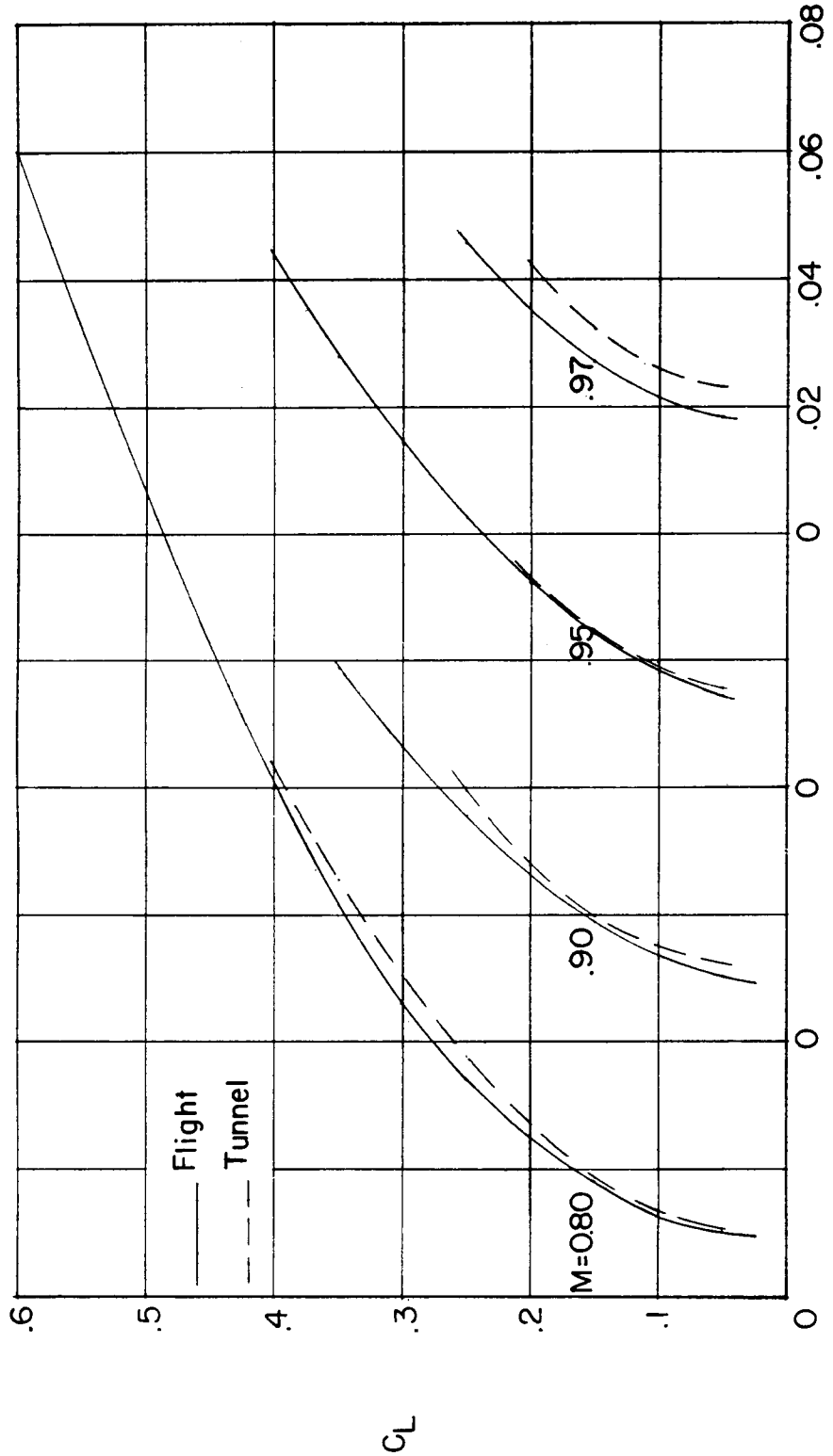

(b) Symmetrical wing.

Figure 19.- Concluded.

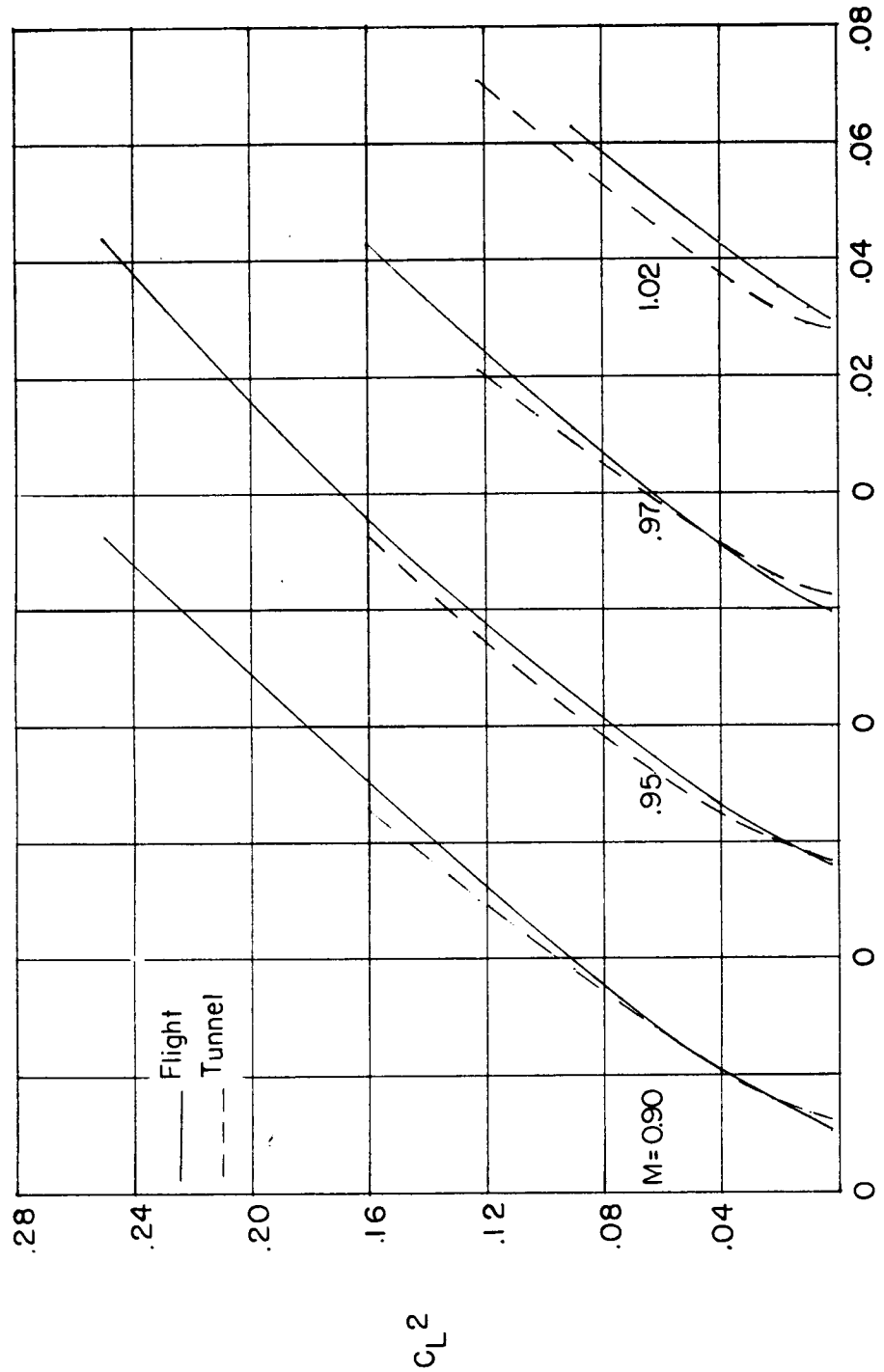

(a) Cambered wing.

Figure 20.- Variation of drag coefficient with lift coefficient squared for several Mach numbers. Trimmed condition.

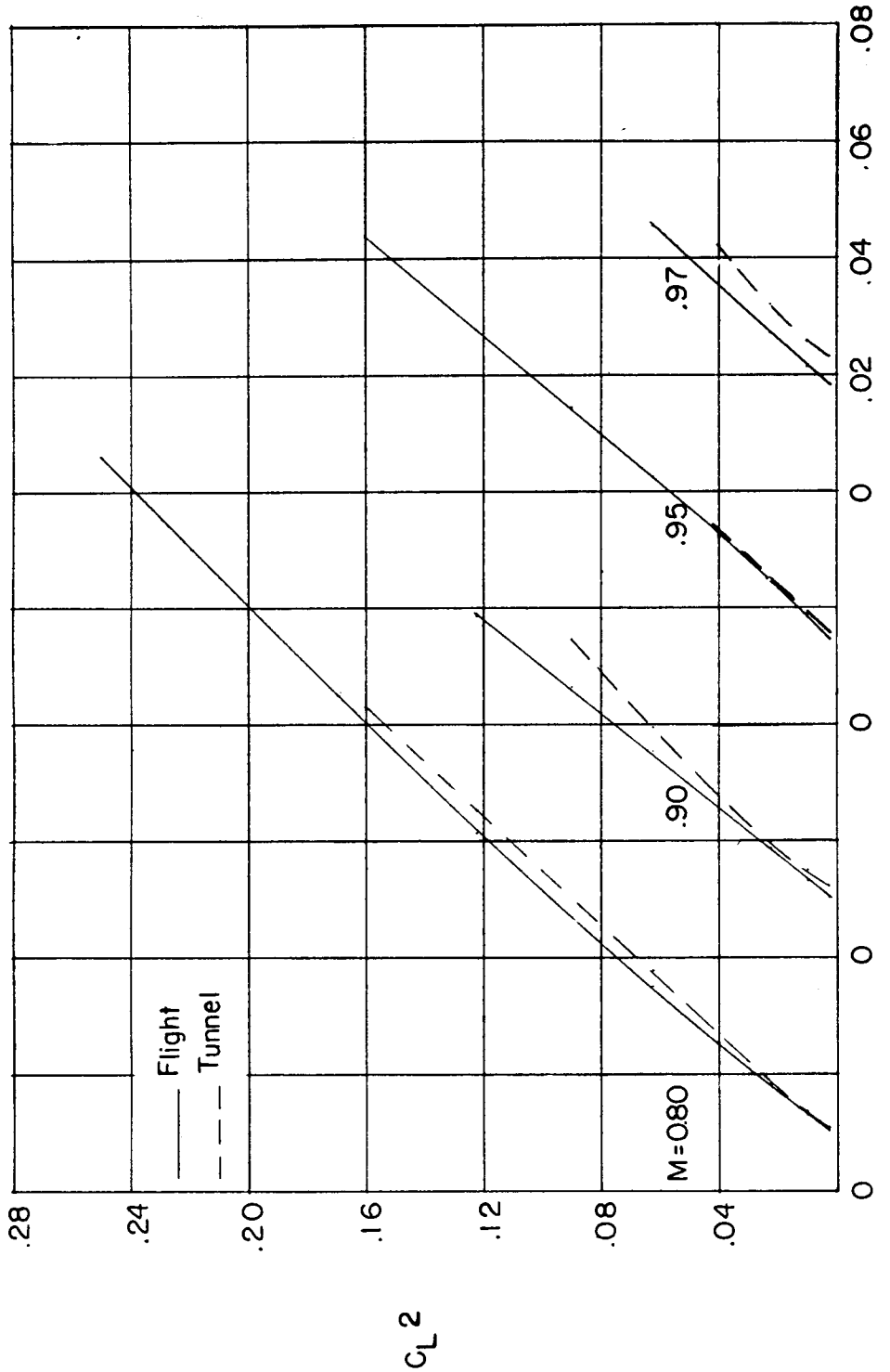

(b) Symmetrical wing.

Figure 20.- Concluded.

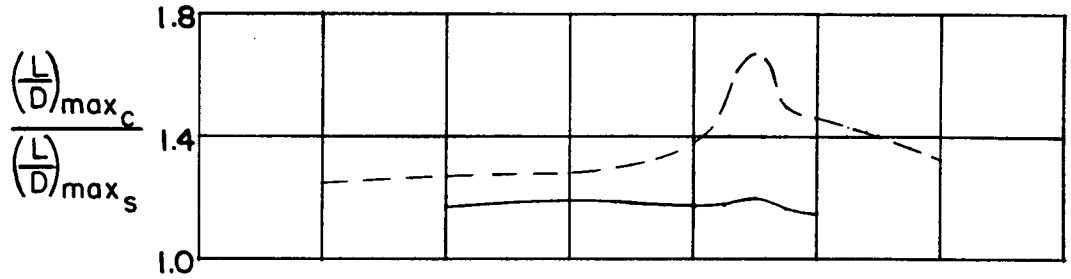

(a) Ratio, cambered to symmetrical.

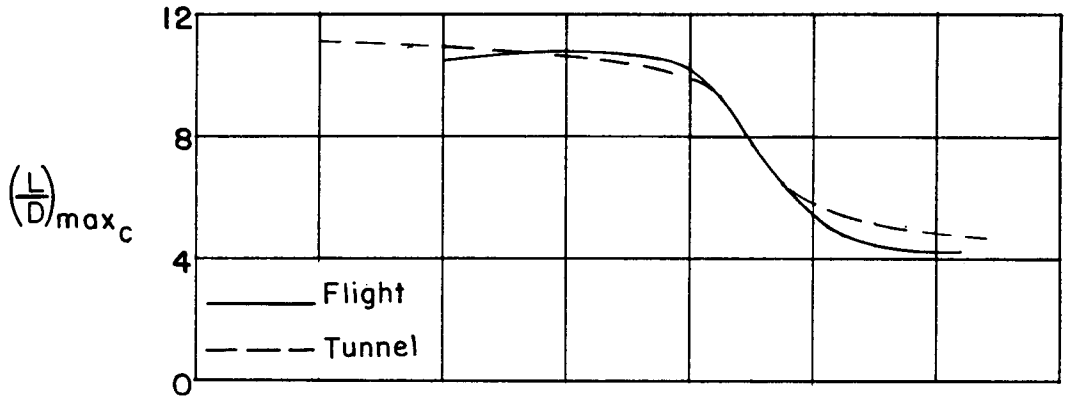

(b) Cambered.

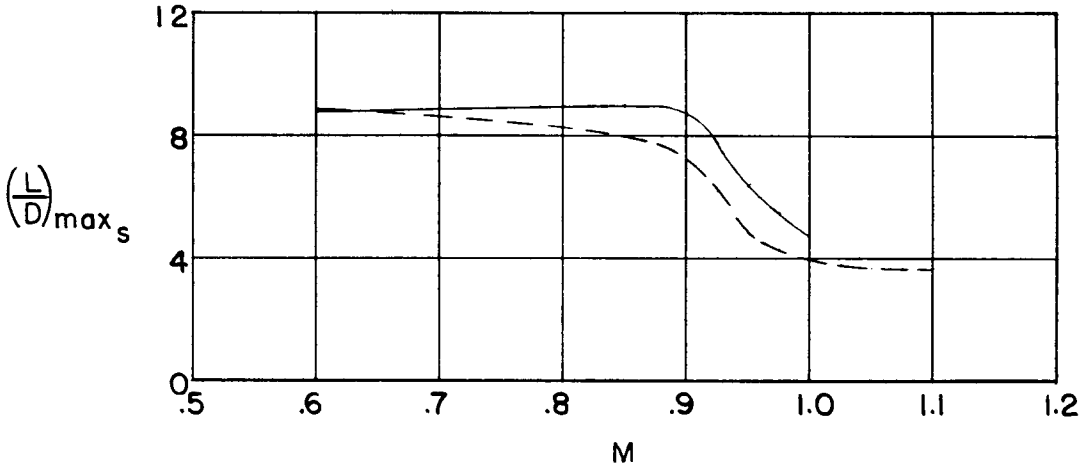

(c) Symmetrical.

Figure 21.- Comparison of maximum lift-drag ratio as measured in flight and wind tunnel. Trimmed condition.

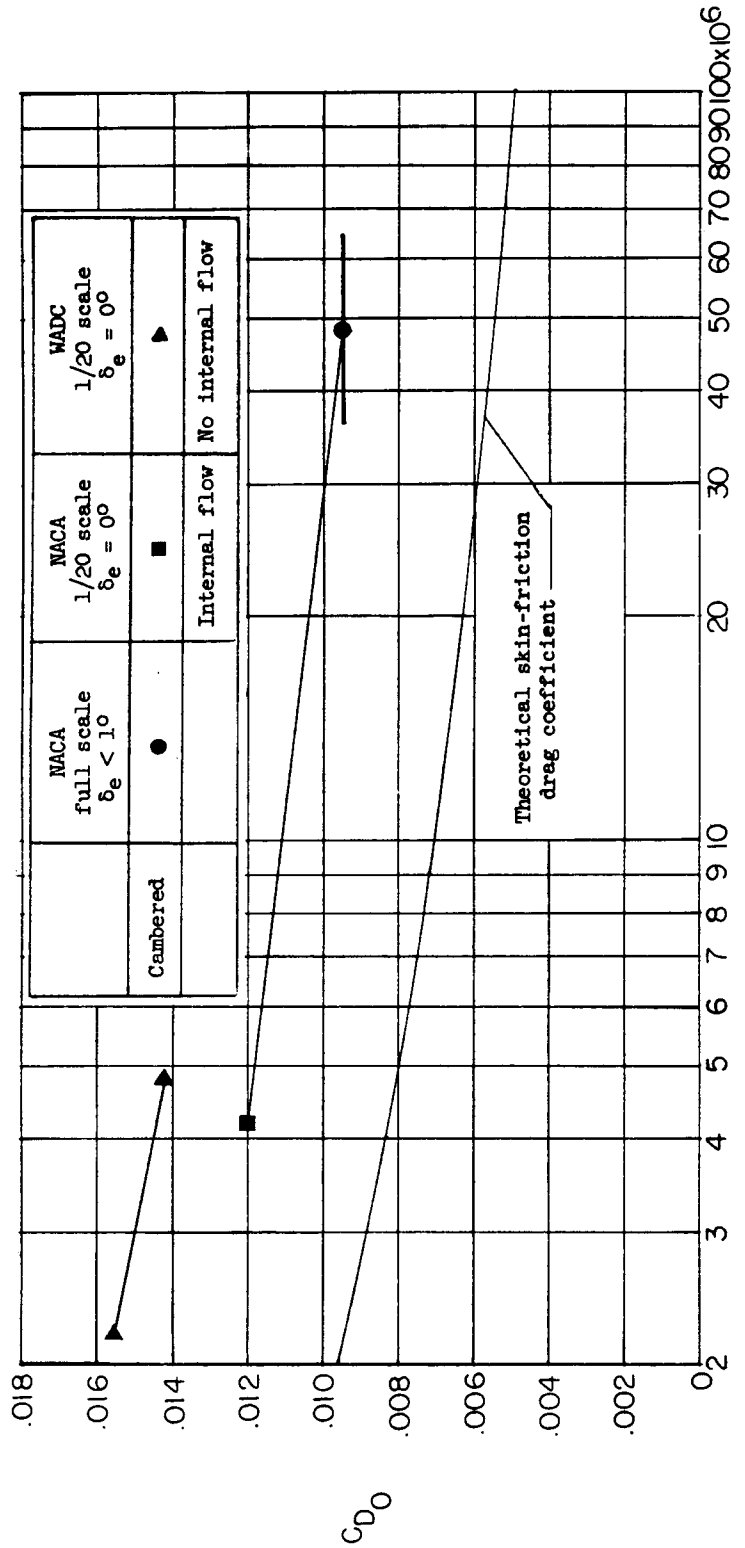

Figure 22.- The relationship of zero-lift drag coefficient and Reynolds number for M = 0.8.